Multiscale Static Analysis of Notched and Unnotched Laminates Using the Generalized Method of Cells

Paria Naghipour Ghezeljeh
Ohio Aerospace Institute, Brook Park, Ohio

Steven M. Arnold and Evan J. Pineda
Glenn Research Center, Cleveland, Ohio

Bertram Stier
Institute of Applied Mechanics, RWTH Aachen University, Aachen, Germany

Lucas Hansen
University of Michigan, Ann Arbor, Michigan

Brett A. Bednarcyk
Glenn Research Center, Cleveland, Ohio

Anthony M. Waas
University of Washington, Seattle, Washington

NASA STI Program . . . in Profile

Since its founding, NASA has been dedicated to the advancement of aeronautics and space science. The NASA Scientific and Technical Information (STI) Program plays a key part in helping NASA maintain this important role.

The NASA STI Program operates under the auspices of the Agency Chief Information Officer. It collects, organizes, provides for archiving, and disseminates NASA's STI. The NASA STI Program provides access to the NASA Technical Report Server—Registered (NTRS Reg) and NASA Technical Report Server—Public (NTRS) thus providing one of the largest collections of aeronautical and space science STI in the world. Results are published in both non-NASA channels and by NASA in the NASA STI Report Series, which includes the following report types:

- TECHNICAL PUBLICATION. Reports of completed research or a major significant phase of research that present the results of NASA programs and include extensive data or theoretical analysis. Includes compilations of significant scientific and technical data and information deemed to be of continuing reference value. NASA counter-part of peer-reviewed formal professional papers, but has less stringent limitations on manuscript length and extent of graphic presentations.

- TECHNICAL MEMORANDUM. Scientific and technical findings that are preliminary or of specialized interest, e.g., "quick-release" reports, working papers, and bibliographies that contain minimal annotation. Does not contain extensive analysis.

- CONTRACTOR REPORT. Scientific and technical findings by NASA-sponsored contractors and grantees.

- CONFERENCE PUBLICATION. Collected papers from scientific and technical conferences, symposia, seminars, or other meetings sponsored or co-sponsored by NASA.

- SPECIAL PUBLICATION. Scientific, technical, or historical information from NASA programs, projects, and missions, often concerned with subjects having substantial public interest.

- TECHNICAL TRANSLATION. English-language translations of foreign scientific and technical material pertinent to NASA's mission.

For more information about the NASA STI program, see the following:

- Access the NASA STI program home page at http://www.sti.nasa.gov

- E-mail your question to help@sti.nasa.gov

- Fax your question to the NASA STI Information Desk at 757-864-6500

- Telephone the NASA STI Information Desk at 757-864-9658

- Write to:
  NASA STI Program
  Mail Stop 148
  NASA Langley Research Center
  Hampton, VA 23681-2199

NASA/TM—2016-219084

Multiscale Static Analysis of Notched and Unnotched Laminates Using the Generalized Method of Cells

Paria Naghipour Ghezeljeh
Ohio Aerospace Institute, Brook Park, Ohio

Steven M. Arnold and Evan J. Pineda
Glenn Research Center, Cleveland, Ohio

Bertram Stier
Institute of Applied Mechanics, RWTH Aachen University, Aachen, Germany

Lucas Hansen
University of Michigan, Ann Arbor, Michigan

Brett A. Bednarcyk
Glenn Research Center, Cleveland, Ohio

Anthony M. Waas
University of Washington, Seattle, Washington

National Aeronautics and
Space Administration

Glenn Research Center
Cleveland, Ohio 44135

August 2016

Acknowledgments

Level of Review: This material has been technically reviewed by technical management.

Available from

Multiscale Static Analysis of Notched and Unnotched Laminates Using the Generalized Method of Cells

Paria Naghipour Ghezeljeh
Ohio Aerospace Institute
Brook Park, Ohio 44142

Steven M. Arnold and Evan J. Pineda
National Aeronautics and Space Administration
Glenn Research Center
Cleveland, Ohio 44135

Bertram Stier
Institute of Applied Mechanics
RWTH Aachen University
Aachen, Germany

Lucas Hansen
University of Michigan
Ann Arbor, Michigan 48109

Brett A. Bednarcyk
National Aeronautics and Space Administration
Glenn Research Center
Cleveland, Ohio 44135

Anthony M. Waas
University of Washington
Seattle, Washington 98195

Summary

The generalized method of cells (GMC) is demonstrated to be a viable micromechanics tool for predicting the deformation and failure response of laminated composites, with and without notches, subjected to tensile and compressive static loading. Given the axial [0], transverse [90], and shear [+45/–45] response of a carbon/epoxy (IM7/977–3) system, the unnotched and notched behavior of three multidirectional layups (Layup 1: $[0,45,90,–45]_{2S}$, Layup 2: $[0,60,0]_{3S}$, and Layup 3: $[30,60,90,–30, –60]_{2S}$) are predicted under both tensile and compressive static loading. Matrix nonlinearity is modeled in two ways. The first assumes all nonlinearity is due to anisotropic progressive damage of the matrix only, which is modeled, using the multiaxial mixed-mode continuum damage model (MMCDM) within GMC. The second utilizes matrix plasticity coupled with brittle final failure based on the maximum principle strain criteria to account for matrix nonlinearity and failure within the FEAMAC software multiscale framework. Both MMCDM and plasticity models incorporate brittle strain- and stress-based failure criteria for the fiber. Upon satisfaction of these criteria, the fiber properties are immediately reduced to a nominal value. The constitutive response for each constituent (fiber and matrix) is characterized using a combination of vendor data and the axial, transverse, and shear responses of unnotched laminates. Then, the capability of the multiscale methodology is assessed by performing blind predictions of the mentioned notched and unnotched composite laminates response under tensile and compressive loading. Tabulated data along with the detailed results (i.e., stress-strain curves as well as damage evolution states at various ratios of strain to failure) for all laminates are presented.

1.0   Introduction

Utilizing micromechanics to capture the progressive damage of carbon-fiber-reinforced polymer (CFRP) composites is of great importance, as most first-ply failure criteria remain insufficient where significant nonlinearity occurs before final failure (Ref. 1). Micromechanics enables one to account explicitly for variations in constituent material properties as well as microstructural effects, such as fiber volume content, packing, and orientation, making it a robust analysis tool for prediction of failure in composites. Moreover, interactive effects between the constituents in the composites are accounted for automatically, rather than through the postulation of an anisotropic continuum damage model.

The generalized method of cells (GMC), first developed by Paley and Aboudi (Ref. 2) and subsequently enhanced (Ref. 3), is analytical in nature, and its formulation involves application of several governing conditions in an average sense. It provides the local fields in composite materials, allowing incorporation of any nonlinear constitutive models (both deformation and damage). The microstructure of a periodic material is represented, within the context of GMC, by a rectangular repeating unit cell (RUC) consisting of an arbitrary number of rectangular subcells, each of which may be a distinct material (Fig. 1). Displacement and traction continuity is enforced in an average, or integral, sense at each of the subcell interfaces and the periodic boundaries of the RUC. These continuity conditions are used to formulate a strain concentration matrix, which gives all the local subcell strains in terms of the global average applied strains. The local subcell stresses can then be calculated using the local constitutive law and the local subcell strains. Finally, the overall RUC stiffness is obtained, utilizing the local constitutive laws and the strain concentration matrix averaged over the RUC dimensions. Various elastic and nonlinear (time-independent plasticity, viscoplasticity, and damage) constitutive models available in the MAC/GMC (Micromechanics Analysis Code with Generalized Method of Cells) software package, developed by NASA Glenn Research Center, facilitate modeling the complex behavior of a composite (Ref. 3). Note that, because of the semi-analytical formulation of the GMC, fully nonlinear solutions (including strain softening) can be efficiently obtained, on the order of seconds. The detailed methodology of GMC and its formulation embedded within classical laminate theory (CLT) is described thoroughly in References 2 and 3.

The multiaxial mixed-mode continuum damage model (MMCDM) was developed by Bednarcyk, Aboudi, and Arnold (Ref. 4). It accounts for the multiaxiality and progressive nature of damage in a constituent material via anisotropic stiffness reduction based on stress-strain curves for the constituent material. Final tensile and shear failure criteria are introduced based on the mode-specific strain energy release rates, and the compression failure criterion is introduced based on a total compressive dissipated strain energy criterion. Previous results by Bednarcyk, Aboudi, and Arnold (Ref. 4) and Pineda, Bednarcyk, and Arnold (Ref. 5) illustrate the flexibility of the MMCDM to capture the vastly different character of the
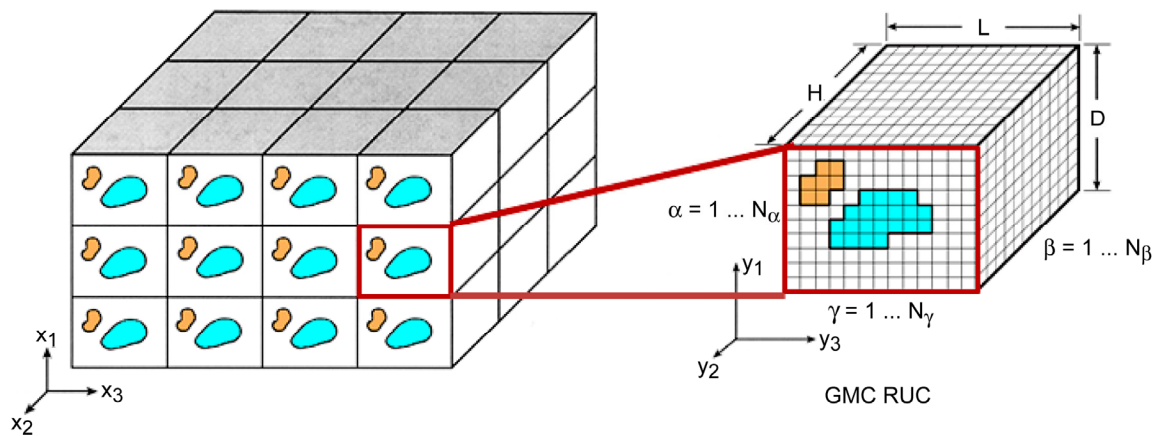
Figure 1.—Composite with repeating unit cell (RUC) microstructure and arbitrary constituents (GMC is Generalized Method of Cells).

monolithic (neat) resin matrix and various multidirectional composites in response to far-field loading. It is noted that the main thesis of the MMCDM model is that nonlinearity in polymer matrices within fiber composite laminae is dictated by microcracking, which is the major source of nonlinearity. Consequently, the unloading stiffness is reduced compared to the loading stiffness (unlike the nonlinearity in metal plasticity, which is associated with accumulation of inelastic strains) and closely related to observed and measured experimental responses (see for example, tests by Sicking (Ref. 6), Schapery and Sicking (Ref. 7), and Lamborn and Schapery (Ref. 8)).

The semi-analytical formulation of GMC and its implementation into MAC/GMC offers significant computational efficiency to obtain the response (e.g., effective properties, global and local (constituent) stress and strain fields) of a volume element of material; consequently, it is unable to model structural details (i.e., complex geometries, cutouts, etc.). Further, GMC is ideal for implementation within a multiscale framework; wherein the higher (structural) scale is modeled using the finite element method (FEM), and the material point response is modeled using GMC. FEAMAC is a synergistic multiscale framework, also developed by NASA Glenn, which couples the micromechanics directly to the FEM and is capable of modeling advanced composite structures (Ref. 9). FEAMAC offers both accuracy and efficiency, at the constituent (fiber and matrix) level and at the global level of a composite structural analysis. In FEAMAC, the micromechanics model (GMC) is called at the desired integration points of the finite element (FE) model (Fig. 2). Any nonlinearity such as plasticity or damage (e.g., MMCDM) in the fiber/matrix constituents at any point in the structure are thus captured locally via an RUC. The RUC is homogenized, and the nonlinear behavior of the constituents within the structure is manifested in the structural response of the FE model. FEAMAC has previously been shown to be fully capable of multiscale, progressive failure analysis of notched CFRP laminates (Ref. 10). More information on FEAMAC, and examples of its fidelity and efficiency as a multiscale analysis tool, is available in Reference 3.

This study was conducted under the support of Phase I of the Air Force Research Laboratory (AFRL) Tech Scout Project (Tech Scout I) aimed at evaluation of existing progressive damage prediction methods. Blind static and fatigue failure predictions were carried out for three different multidirectional laminates (Layup 1: $[0,45,90,-45]_{2S}$; Layup 2: $[0,60,0]_{3S}$; and Layup 3: $[30,60,90,-30,-60]_{2S}$) throughout the project timeline. This work demonstrates the application of MAC/GMC, utilizing both MMCDM and plasticity to model the constitutive response of the GMC matrix subcells, as an ultra-efficient analysis tool to simulate tensile and compressive failure of unnotched, multidirectional carbon/epoxy IM7/977–3 composite layups. A multiscale framework is required to model structural features such as notches. Since MMCDM was not fully implemented in the FEAMAC framework before the due date of the blind
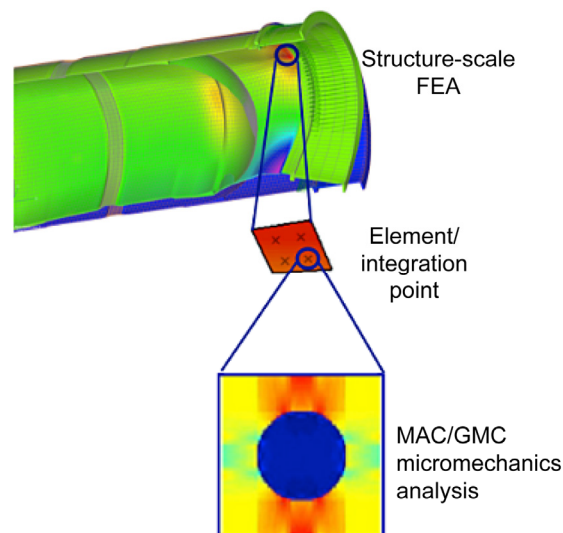
Figure 2.—Implementation of FEAMAC code within Abaqus built-in UMAT framework (MAC/GMC is Micromechanics Analysis Code with Generalized Method of Cells).

predictions, incremental J2 plasticity theory was used in FEAMAC as an alternative to predict the nonlinear response of the matrix subcells within notched coupons subjected to tensile and compressive loading (Ref. 11). A maximum strain criterion was used to capture failure within the matrix subcells of the FEAMAC-plasticity models. Upon satisfaction of this criterion in any of the matrix subcells, the elastic properties of that subcell are completely diminished. This failure methodology was also used for the fiber subcells (which were assumed to exhibit no nonlinearity prior to failure) in both the MAC/GMC-MMCDM and FEAMAC-plasticity models. For completeness, the unnotched coupons were also modeled using the FEAMAC-plasticity strategy.

The constitutive models used in the blind predictions were characterized and/or calibrated from experimental unnotched coupon data analysis (i.e., [0], [90], and [±45] laminates). All experimental data used in this manuscript were obtained by AFRL. Please refer to Reference 11 for details on the experimental and programmatic components of the Tech Scout I. After submission of blind predictions, the models were recalibrated to better correlate to the validation experiments as part of Tech Scout I. Subsequently, after the conclusion of Tech Scout I, additional FE dimensionality and mesh density studies were performed. Tabulated results and stress-strain curves for all predictions of three multidirectional layups along with the recalibrations are presented here.

2.0   Matrix Constituent Constitutive Models Used

Herein the two matrix constitutive models used will be presented. For clarity the subcell elimination (SE) method is used to mimic failure in the constituents of a RUC within MAC/GMC. Upon satisfaction of a failure criterion, all components of the stiffness matrix of the subcell are multiplied by $1 - D^{max}$. For the simulations presented in this work, $D^{max} = 0.9999$. Upon elimination of a subcell, that subcell can no longer carry any substantial stress. It should be noted, though, the SE method can result in pathological dependence of the solution on the FE mesh density in a multiscale simulation where GMC is coupled to FEM.

2.1   Multiaxial Mixed-Mode Continuum Damage Model

The MMCDM (Ref. 4) assumes that damage initiation in each subcell is determined using quadratic definitions of damage strains, a three-dimensional (3D) extension of the strain-based Hashin criterion:

$$\varepsilon_1^D = \sqrt{\left(\frac{\varepsilon_{11}'}{X_\varepsilon}\right)^2 + \left(\frac{\gamma_{13}'}{R_\varepsilon}\right)^2 + \left(\frac{\gamma_{12}'}{S_\varepsilon}\right)^2}$$

$$\varepsilon_2^D = \sqrt{\left(\frac{\varepsilon_{22}'}{Y_\varepsilon}\right)^2 + \left(\frac{\gamma_{23}'}{Q_\varepsilon}\right)^2 + \left(\frac{\gamma_{12}'}{S_\varepsilon}\right)^2} \tag{1}$$

$$\varepsilon_3^D = \sqrt{\left(\frac{\varepsilon_{33}'}{Z_\varepsilon}\right)^2 + \left(\frac{\gamma_{23}'}{Q_\varepsilon}\right)^2 + \left(\frac{\gamma_{13}'}{R_\varepsilon}\right)^2}$$

where ε_i^D is damage initiation strain; ε_{ij}' is total strain; γ_{ij}' is total shear strain; and X_ε, Y_ε, Z_ε, Q_ε, R_ε, and S_ε are strain allowables. Damage is initiated when any of the specified directional equations (Eq. (1)) are greater than or equal to zero. Once the damage is initiated, the tangent stiffness k_i of the damage stress-versus-damage-strain curve (Fig. 3) is used to control the damage evolution law (D_i is the damage variable)

$$dD_i = \left(1 - D_i - k_i'\right)\frac{d\varepsilon_i^D}{\varepsilon_i^D} \tag{2}$$
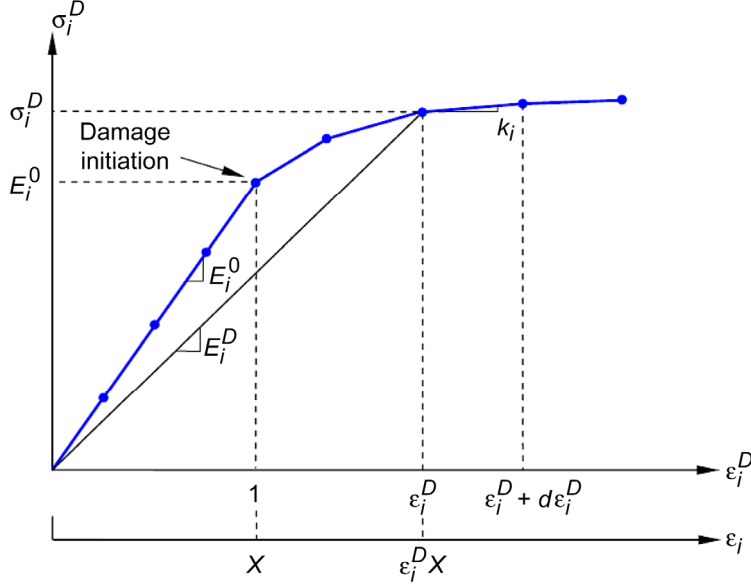
Figure 3.—Stress-strain curve utilized in the multiaxial mixed-mode continuum damage model (MMCDM), showing damage evolution (σ_i^D is incremental stress, E_i^0 is initial elastic modulus, E_i^D is incremental elastic modulus, ε_i^D is incremental strain, and k_i is normalized tangent stiffness).

The normalized tangent stiffness k_i' is given in exponential form:

$$k_i' = A e^{-\varepsilon_i^D / B} \tag{3}$$

Once the damage variable is determined, the individual elastic material properties can be degraded (where b_{ij} are individual damage weighting factors):

$$
\begin{aligned}
E_1 &= (1 - b_{11}D_1)E_1^0 & \nu_{12} &= (1 - b_{11}D_1)\nu_{12}^0 & G_{12} &= (1 - b_{61}D_1 - b_{62}D_2)G_{12}^0 \\
E_2 &= (1 - b_{22}D_2)E_2^0 & \nu_{13} &= (1 - b_{11}D_1)\nu_{13}^0 & G_{13} &= (1 - b_{51}D_1 - b_{53}D_3)G_{13}^0 \\
E_3 &= (1 - b_{33}D_3)E_3^0 & \nu_{23} &= (1 - b_{22}D_2)\nu_{23}^0 & G_{23} &= (1 - b_{42}D_2 - b_{43}D_3)G_{23}^0
\end{aligned}
\tag{4}
$$

where ε_{ij} is elastic modulus, ν_{ij} is Poisson's ratio, and G_{ij} is shear modulus.

With the MMCDM a mixed-mode fracture criterion is used to determine the final failure. Upon satisfaction of the ith criterion the D_i damage variable is set to a value very close to 1. Note that in the previous work of Bednarcyk, Aboudi, and Arnold (Ref. 4) the characteristic lengths used to calculate the mode-specific strain energy release rates, G_k, were specified as a material property. Yet in the new implementation of the ImMAC suite used within this paper, they can be controlled by the actual subcell dimensions. Three mixed-mode criteria are available: (1) maximum strain energy release rate, (2) mixed-mode power law, or (3) the Benzeggagh-Kenane (B-K) criterion. In this work, the mixed-mode power law criterion is assumed:

$$\left(\frac{G_I^i}{G_I^C}\right)^\alpha + \left(\frac{G_{II}^i}{G_{II}^C}\right)^\alpha + \left(\frac{G_{III}^i}{G_{III}^C}\right)^\alpha = 1 \tag{5}$$
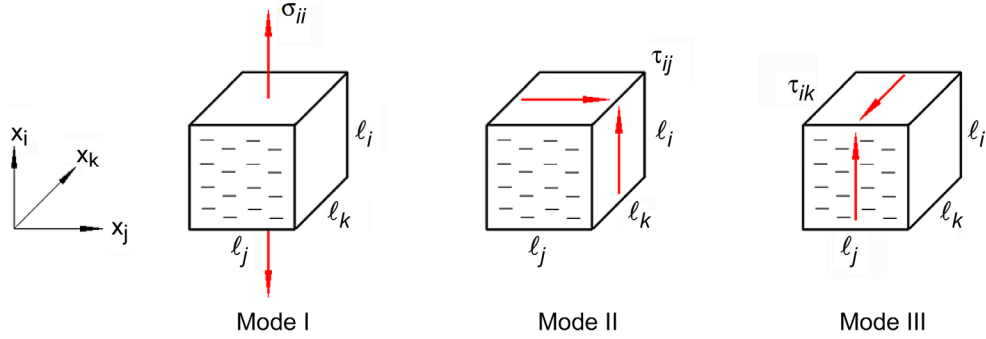
Figure 4.—Three fracture modes in x-coordinate frame (σ_{ii} is normal stress, τ_{ij} is shear stress (mode II), τ_{ik} is shear stress (mode III), and ℓ is characteristic element length).

Here, G_M^i is the strain energy release rate under tension for a mode M crack perpendicular to the i-direction, and G_M^c is the mode M fracture toughness where M = I, II, or III (Fig. 4).

It is also assumed that cracks cannot grow under compression. So, for a normal compressive load, a maximum strain energy criterion is used for final failure (W_s^C = critical strain energy), which is determined from increments of the mode-specific strain energy release rates $\left(W_\mathrm{I}^i, W_\mathrm{II}^i, W_\mathrm{III}^i\right)$ over the RUC volume:

$$W_\mathrm{I}^i + W_\mathrm{II}^i + W_\mathrm{III}^i = W_s^C \tag{6}$$

The reader is referred to Bednarcyk, Aboudi, and Arnold (Ref. 4) for the derivations of G_i and W_i used in Equations (5) and (6), respectively.

2.2 Classical Plasticity

Plasticity theory assumes energy is dissipated through dislocation motion, resulting in permanent plastic strain. In this study, when plasticity is used the assumption is that microdamage and inelastic material behavior follow the same evolution law as dislocation motion in metals observe. In the classical theory of plasticity, the increment in the plastic strain component $\Delta\varepsilon_{ij}^p$ is given by

$$\Delta\varepsilon_{ij}^p = \Delta\lambda\left(\frac{\mathrm{d}f}{\mathrm{d}\sigma_{ij}}\right) \tag{7}$$

where f is a defined yield function based on J$_2$ plasticity theory and $\Delta\lambda$ is the proportionality factor. This theory is implemented in the MAC/GMC framework through the radial return algorithm, keeping the stress state on the evolving yield surface while plastic stress is accumulating (see Aboudi, Arnold, and Bednarcyk (Ref. 3)).

3.0 Characterization and Calibration

Unnotched [0], [90], and $[\pm 45]_{4s}$ coupon experimental data were provided by the AFRL Tech Scout Project (Ref. 11) and used to calibrate the MMCDM-SE and Plasticity-SE models within MAC/GMC.

3.1 MAC/GMC With MMCDM-SE

The elastic properties of fiber and matrix (Table I) were obtained from vendor data or were partially backed out from elastic lamina properties measured for IM7/977–3. A fiber volume fraction of 65 percent was used. The 7-by-7 doubly-periodic, square-packed RUC (shown in Fig. 5(a), which represents continuous reinforcement) was used for analyzing the composite material. The matrix was assumed isotropic with a Young's modulus E_m and a Poisson's ratio ν_m. The fiber was assumed to behave transversely isotropic, where E_{f11} is the longitudinal modulus, E_{f22} is the transverse modulus, ν_{f12} is the longitudinal Poisson's ratio and G_{f12} is the longitudinal shear modulus. CLT (see Fig. 5(b)) within MAC/GMC was used to model all unnotched laminates, including the characterization coupons, wherein the RUC represented in Figure 5(a) provides the constitutive response of the integration points within each layer.

TABLE I.—CONSTITUENT PROPERTIES AND INPUT PARAMETERS
USED TO CALIBRATE MMCDM-SE MODEL FOR
IM7/977–3 CARBON FIBER/EPOXY LAMINATE

(a) Properties	(b) Parameters
Longitudinal modulus (fiber) E^T_{f11} = 276 GPa (tension) E^C_{f11} = 215 GPa (compression)	Strain allowable X^T_ε = 0.012 (tension) X^C_ε = 0.0337 (compression) S_ε = 0.0253 (shear)
Transverse modulus (fiber) E_{f22} = 16 GPa	Damage coefficient, exponent $A^T = 1$, $B^T = 3.25$ (tension) $A^C = 1$, $B^C = 2.5$ (compression)
Longitudinal Poisson's ratio (fiber) ν_{f12} = 0.31	Damage weighting factor $b^T_{22} = 2$, $b^T_{ii} = 1$ ($i \neq 2$) (tension) $b^C_{ii} = 1$, $b_{4i} = b_{5i} = b_{6i} = 0.5$ (compression)
Transverse Poisson's ratio (fiber) ν_{f23} = 0.28	Ultimate fiber strain $\varepsilon^{T,\text{ult}}_f$ = 0.0161 (tension) $\varepsilon^{C,\text{ult}}_f$ = 0.0098 (compression)
Shear modulus (fiber) G_{f12} = 15 GPa	Strain energy release rate (tension) G^c_{I} = 6 J/m² (mode I) $G^c_{\text{II}} = G^c_{\text{III}} = 250e^3$ J/m² (modes II and III)
Young's modulus (matrix) E_m = 3.5 GPa	
Poisson's ratio (matrix) ν_m = 0.35	Critical strain energy (compression) $W^C_s = 5.55e^{-6}$ J/m²
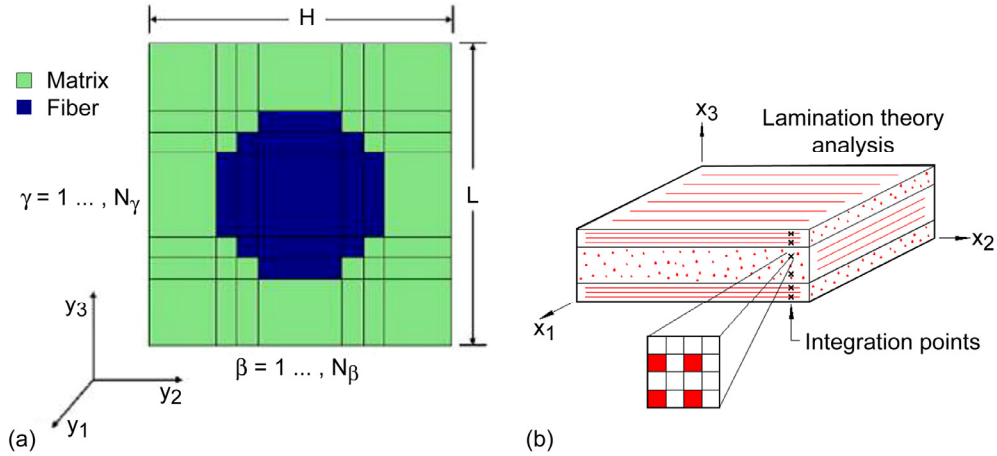
Figure 5.—Square-packed 7-by-7 repeating unit cell (RUC) definition for carbon fiber composite laminate. (a) Standalone. Blue subcells represent fiber, and green subcells represent matrix. (b) Classical laminate theory (CLT) within Micromechanics Analysis Code with Generalized Method of Cells (MAC/GMC).

Data from three uniaxial coupon tests—longitudinal tension ([0]8) and compression ([0]16), transverse tension ([90]16) and compression ([90]24), and shear ([±45]4s)—were used to calibrate the MMCDM-SE model parameters within MAC/GMC (where T and C indicate tension and compression, respectively): S_ε, A^T, B^T, G_{II}^C, and G_{III}^C from the shear test; X_ε^C, A^c, B^c, and W_s^C from the transverse compression test; and X_ε^T and G_I^C from the transverse tension test. All of the parameters calibrated for the MMCDM-SE model, together with above-mentioned constituent properties, are summarized in Table I. For fiber failure, the SE method was used. A maximum normal strain criterion, with different critical strains in tension and compression based on 0° tension and compression tests ($\varepsilon_{\text{fiber}}^{\text{ult}}$), was employed. The detailed definition of the MMCDM-SE properties listed in Table I can be found in Section 2.1.

3.2   FEAMAC with Plasticity-SE

The plasticity-SE model was calibrated similar to the way MMCDM-SE was by using the provided unnotched [0], [90], and [±45]4s coupon experimental data and a single RUC within MAC/GMC. The same elastic properties for the constituents and critical fiber strains were used as in MMCDM-SE; however, for the case of Plasticity-SE the same value for the longitudinal modulus of the fiber in tension and in compression (276 GPa) was employed. Furthermore, data from the [±45°]4S laminate were used to characterize the effective nonlinear stress-strain response of the matrix. A tabulated form of this effective stress-strain curve (Fig. 6) was used directly in MAC/GMC and FEAMAC to dictate the strain hardening behavior of the matrix subcells.

To capture matrix failure, the SE method was used. A strain-based failure criterion, with different allowables in tension, $\varepsilon_m^{\text{ult}}$, and in shear, γ_m^{ult}, (based on transverse and shear tensile tests, respectively) was employed to mark the end of the local stress-strain curve. Table II summarizes the complete list of unique model parameters and properties used to calibrate the Plasticity-SE theory.
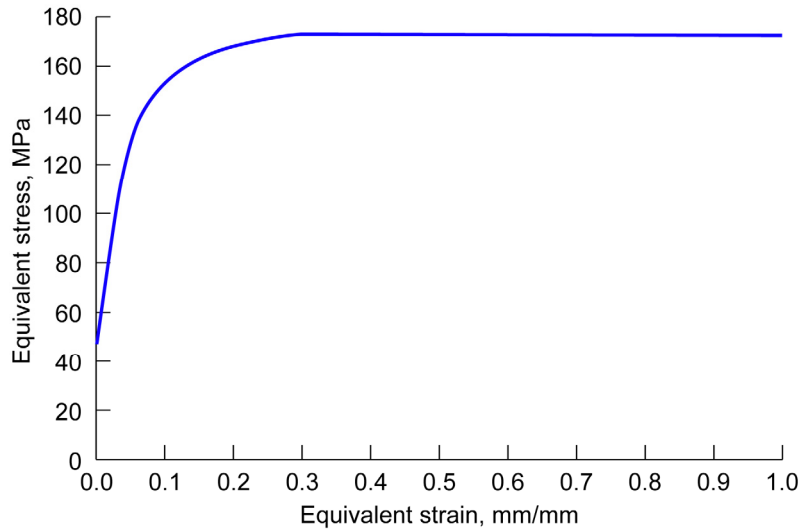
Figure 6.—Characterization of effective nonlinear stress-strain response of 977–3 epoxy matrix.

TABLE II.—CONSTITUENT PROPERTIES AND INPUT PARAMETERS
USED TO CALIBRATE PLASTICITY-SE MODEL FOR
IM7/977–3 CARBON FIBER/EPOXY LAMINATE

(a) Properties	(b) Parameters
Longitudinal modulus (fiber) E_{f11} = 276 GPa (tension and compression)	Ultimate fiber strain $\varepsilon_f^{T,\text{ult}}$ = 0.0161 (tension) $\varepsilon_f^{C,\text{ult}}$ = 0.0098 (compression)
Transverse modulus (fiber) E_{f22} = 15 GPA	
Longitudinal Poisson's ratio (fiber) ν_{f12} = 0.28	Fiber volume fraction V_f = 67 percent
Transverse Poisson's ratio (fiber) ν_{f23} = 0.19	Ultimate matrix strain $\varepsilon_m^{\text{ult}}$ = 0.0139
Shear modulus (fiber) G_{f12} = 15 GPa	
Young's modulus (matrix) E_m = 3.2 GPa	Ultimate shear strain γ_m^{ult} = 0.06
Poisson's ratio (matrix) ν_m = 0.38	Yield strength σ_y = 48.3 MPa

3.3 Characterization and Calibration Results

The resulting uniaxial stress-strain curves for the above-mentioned 0°, 90°, and ±45° laminates, using both MMCDM-SE and Plasticity-SE within MAC/GMC, are presented in Figure 7. Both MMCDM-SE and Plasticity-SE were able to correlate very well for all three laminates, especially with MMCDM-SE capturing the highly nonlinear shear and transverse compression behavior.
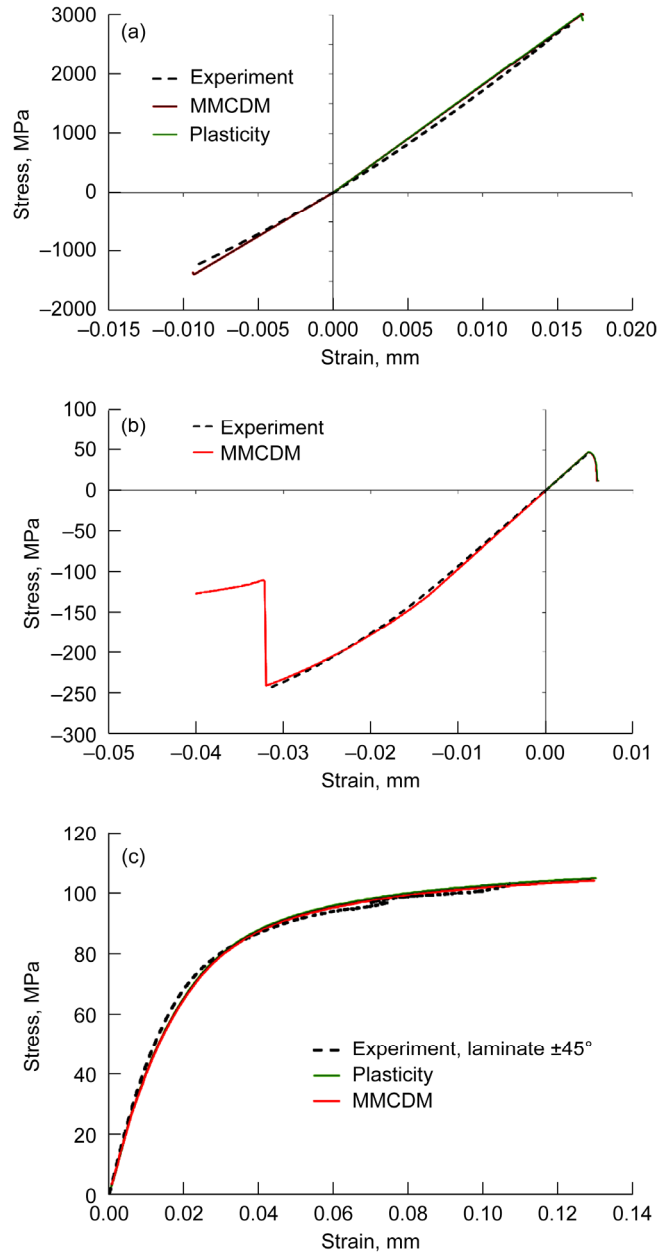
Figure 7.—Predicted uniaxial stress-strain curve for IM7/977–3 carbon-fiber-reinforced epoxy composite laminates from MMCDM-SE and Plasticity-SE models within Micromechanics Analysis Code with Generalized Method of Cells (MAC/GMC) software compared to experiment. (a) $[0]_8$ (longitudinal tension) and $[0]_{16}$ (longitudinal compression). (b) $[90]_{16}$ (transverse tension) and $[90]_{24}$ (transverse compression); transverse response calibrated only with MMCDM-SE. (c) $[\pm45]4s$.

4.0   Results

Resulting uniaxial stress-strain curves for Layups 1, 2, and 3 using MMCDM-SE and Plasticity-SE are presented in this section.

4.1   Unnotched Laminate

In these simulations, it is understood that failure in laboratory coupons is caused by lack of uniformity in both strength and stiffness. That is, in an unnotched coupon, the stiffness is controlled by the variations in material properties and flaws from point to point (departures from the average values), and strength is controlled by which point in the coupon is most likely to fail first. Because there is no "hardening" response in a composite upon failure initiation, unlike in a metal, the deformation localizes, which causes unloading elsewhere in the specimen gage. Because of this, the predictions of strengths in unnotched coupons and comparisons against corresponding experiments are somewhat arduous. Notched coupons, though, provide a clear location where failure mechanisms are likely to occur because of elevated stress states, making comparisons between predictions and experimental results clearer and more meaningful, as addressed later in this report.

The calibrated properties (Tables I and II) were used to predict the failure response of three different unnotched multidirectional layups utilizing MMCDM-SE within MAC/GMC (microscale) and Plasticity-SE within FEAMAC (multiscale). Note standalone MAC/GMC is a more useful tool for unnotched coupon laminates than FEAMAC is, since there is no need for a specific localization strategy, there are no size effects, and the analysis is completed in seconds rather than minutes or hours. Here, the obtained blind stress-strain predictions for all three layups will be described in detail. Meanwhile, three pointwise properties obtained using MAC/GMC-MMCDM-SE are tabulated for all three layups in Section 4.1.5: stiffness, maximum stress, and failure strain.

4.1.1   Blind Predictions (MMCDM-SE)

MMCDM-SE for matrix subcells, and SE for the fiber subcells within MAC/GMC (see Fig. 5) was utilized to simulate the tensile response and failure of the unnotched layups; the calibrated model parameters listed in Table I were used as input. A uniform fiber volume fraction of 65 percent was assumed for all three layups. The resulting ultimate strengths for the three layups under tension were overpredicted with a 19.3-percent error (Layup 1), 2-percent error (Layup 2), and 66.8-percent error (Layup 3). The significant overprediction in Layup 3 can be attributed to the off-axis plies continuing to carry load after failure in the RUC (see Fig. 8). The initial stiffness was overpredicted by 11.5, 13.4, and 10.4 percent for Layups 1, 2, and 3, respectively. Horizontal dashed lines in the figures designate the lower and upper confidence 90 to 95 percent bounds for all the reported experimental results.

Under compression loading, the laminate strength was generally underpredicted, while the stiffness was overpredicted. The largest discrepancy appears in laminates with 0° plies. This was due to the initially low axial compression strength (1274 MPa) reported by AFRL (Ref. 11), which is much lower than previous experimental results (~1680 MPa, Ref. 11) for the same class of materials. Meanwhile, the axial compressive strength of the fiber was increased accordingly to improve the laminate strength predictions later in the recalibration phase. Nonlinearity under compression is attributed to kink-band formation (Refs. 12 and 13). This mechanism is also not captured in the initial predictions, but is addressed successfully in the upcoming recalibration section (Sec. 4.1.2).
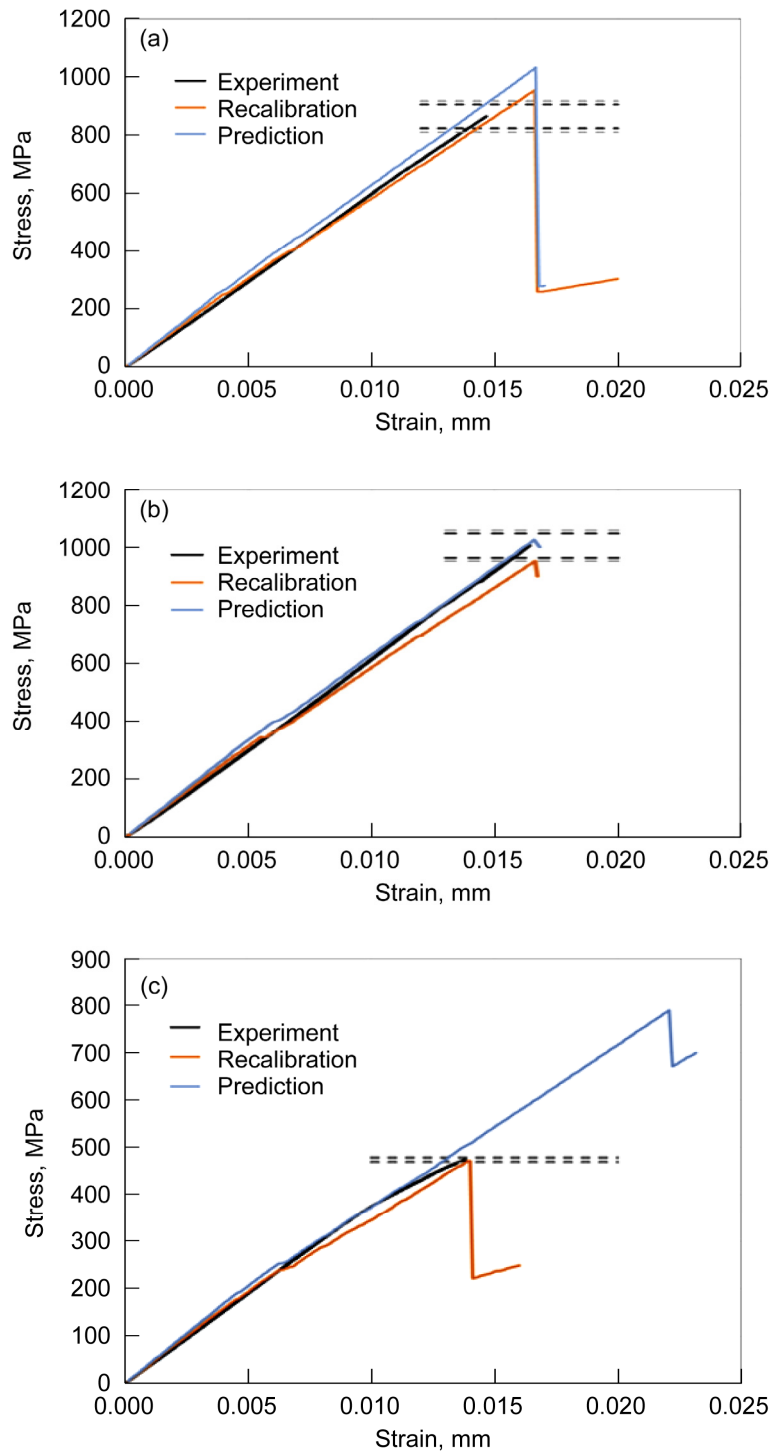
Figure 8.—Tension of unnotched IM7/977–3 carbon-fiber-reinforced epoxy composite laminates predicted and recalibrated using MMCDM-SE model within MAC/GMC software. (a) Layup 1: [0,45,90,–45]$_{2S}$. (b) Layup 2: [0,60,0]$_{3S}$. (c) Layup 3: [30,60,90,–30,–60]$_{2S}$.

4.1.2 Recalibration (MMCDM-SE)

During the recalibration phase, four modifications were made to improve the results obtained using MAC/GMC with MMCDM-SE:

(1) The fiber failure criterion was changed from maximum strain to a "Hashin"-like failure criterion, which incorporated a shear strain component, and a shear strain allowable (X_{fiber} (shear) = 0.003). This was necessary to eliminate latent load-carrying capability of off-axis plies subsequent to matrix failure in tension, a deficiency resulting from utilizing CLT.

(2) Under compression the fiber was modeled using MMCDM-SE to account for apparent toughness due to kink-band formation. Once the damage is initiated (X_{fiber} (compression) = 0.0075), the tangent stiffness of the stress-strain curve (see Fig. 3, Sec. 2.1) is used to control the nonlinear damage evolution law with slope parameters (A_{fiber}, B_{fiber}).

(3) The compressive strength value of the fiber was increased, and the longitudinal stiffness value (in compression) of the fiber was decreased accordingly, to match the recommended values in the literature.

(4) The fiber volume fraction was assumed to be in the lower-bound data provided by AFRL, and it was decreased from 65 to 62 percent to improve stiffness predictions. The parameters used in MMCDM-SE for the recalibration phase are shown in Table III (recalibration modifications are indicated).

Figures 8 and 9 show the blind predictions and recalibrated responses together with experimental results for the aforementioned unnotched layups for both tension and compression loading, respectively. For tension (see Fig. 8), recalibration improved the initial stiffness prediction, and except for a small

TABLE III.—CONSTITUENT PROPERTIES AND INPUT PARAMETERS
USED TO RECALIBRATE MMCDM-SE MODEL FOR IM7/977–3
CARBON FIBER/EPOXY LAMINATE

(a) Properties	(b) Parameters
Longitudinal modulus (fiber) E_{f11}^T = 276 GPa (tension)[a] E_{f11}^T = 215 GPa (compression)	Strain allowable X_ε^T = 0.012 (tension) X_ε^C = 0.0337 (compression) S_ε = 0.0253 (shear)
	Damage coefficient (matrix), exponent A_m^T = 1, B_m^T = 3.25 (tension) A_m^C = 1, B_m^C = 2.5 (compression)
Transverse modulus (fiber) E_{f22} = 16 GPa	Damage weighting factor b_{22}^T = 2, b_{ii}^T = 1 ($i \neq 2$) (tension) b_{ii}^C =1, $b_{4i} = b_{5i} = b_{6i}$ = 0.5 (compression)
Longitudinal Poisson's ratio (fiber) ν_{f12} = 0.31	Strain allowable (fiber) $X_{f\varepsilon}^T$ = 0.0161 (tension)[a]
Transverse Poisson's ratio (fiber) ν_{f23} = 0.28	$X_{f\varepsilon}^S$ = 0.003 (shear)[a] $X_{f\varepsilon}^C$ = 0.0075 (compression)[a]
Shear modulus (fiber) G_{f12} = 15 GPa	Damage coefficient (fiber), exponent A_f^C =1,[a] B_f^C = 4.5[a] (compression)
	Critical strain energy (fiber)[a] $W_{s,f}^C$ = 1.66e^{-5} J/m^2 (compression)
Young's modulus (matrix) E_m = 3.5 GPa	Strain energy release rate (tension) G_I^c = 6 J/m^2 (mode I) $G_{II}^c = G_{III}^c$ = 250e^3 J/m^2 (modes II and III)
Poisson's ratio (matrix) ν_m = 0.35	Critical strain energy (matrix) $W_{s,m}^C$ = 5.55e^{-6} J/m^2 (compression)

[a]Entry was changed for recalibration.

reduction in strength prediction for Layup 2 under tension, the strength results for the other two layups were significantly improved: the relative error in strength prediction was reduced from 72 to 0.4 percent for Layup 3, and from 20 to 10 percent for Layup 1 (see Sec. 4.1.5 for details). Similarly, as shown in Figure 9, recalibration significantly improved both stiffness and strength results for the compression case, successfully capturing the observed experimental nonlinear response. It should be noted that the maximum runtime for the MMCDM-SE simulations was approximately 8.5 s using a single central processing unit (CPU).
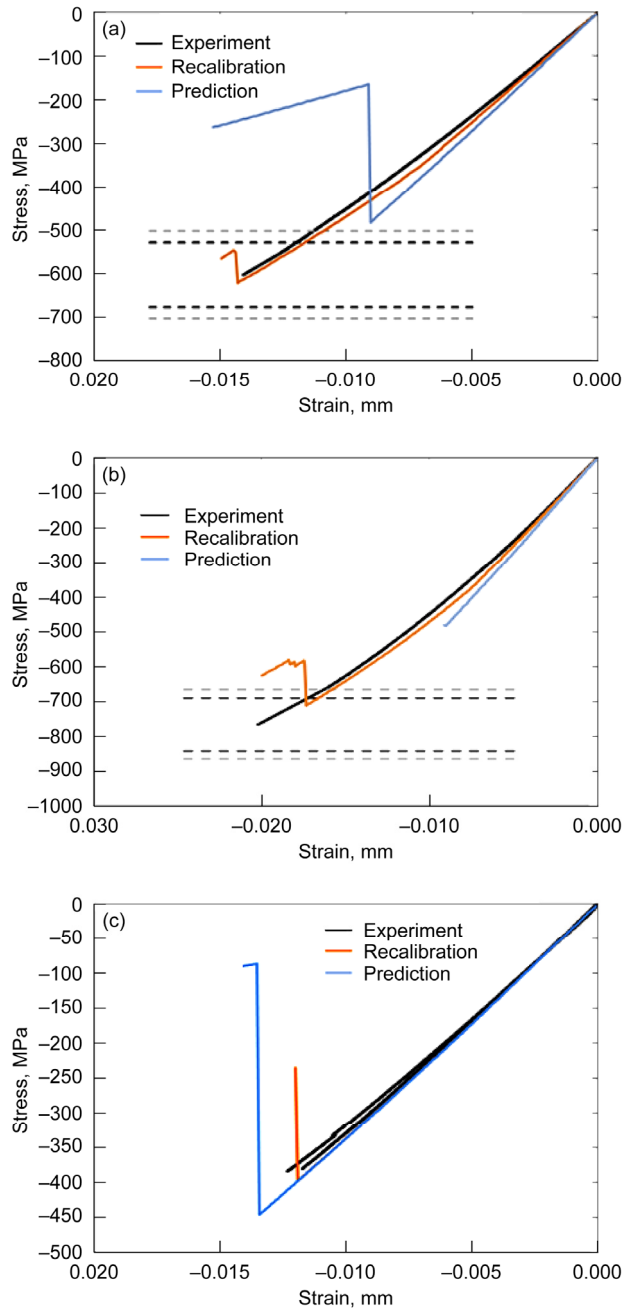
Figure 9.—Compression of unnotched IM7/977–3 carbon-fiber-reinforced epoxy composite laminates predicted and recalibrated using MMCDM-SE model within MAC/GMC software. (a) Layup 1: [0,45,90,–45]$_{2S}$. (b) Layup 2: [0,60,0]$_{3S}$. (c) Layup 3: [30,60,90,–30,–60]$_{2S}$.
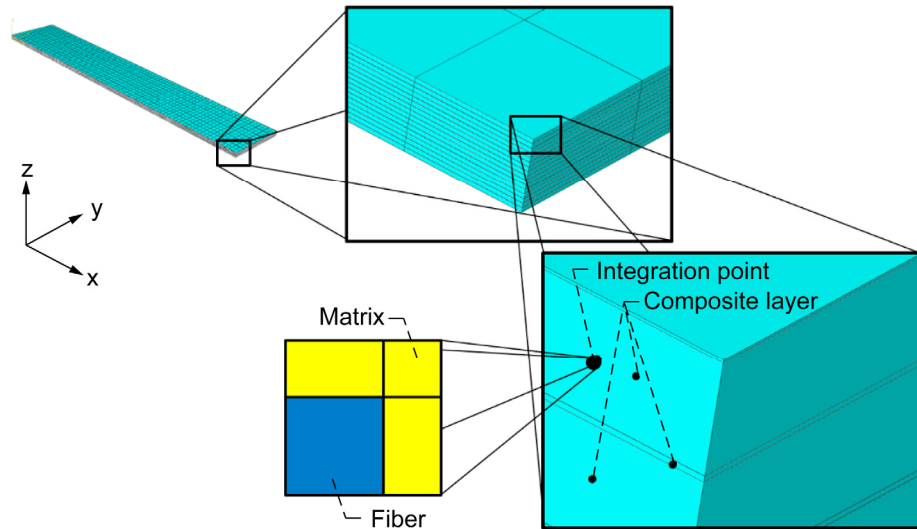
Figure 10.—GMC finite element mesh of unnotched IM7/977–3 carbon-fiber-reinforced epoxy composite laminate to be used within FEAMAC software.

4.1.3 Predictions (Plasticity-SE)

Figure 10 shows an unnotched laminate FE mesh idealization to be used in conjunction with the FEAMAC framework; wherein GMC is called at each integration point of the composite ply within the Abaqus (Ref. 14) FE model. Here a full 3D FE mesh was used, wherein each ply of the composite is discretized through the thickness using a single solid (linear 3D) element. Between each fiber-reinforced layer, a finite-thickness cohesive zone layer was incorporated using cohesive elements to account for delamination. The use of solid elements is deemed suitable for this problem, as the bending in the laminates is negligible. However, using solid elements with only one integration point per element in the thickness direction may be a source of error in capturing the through-thickness stresses needed for accurate delamination. This issue will be addressed in future studies. The cohesive elements represent matrix-rich regions resulting from processing and were assumed to be a linear elastic continuum prior to damage initiation (τ_1 and τ_2 representing mode I and mode II strength, respectively, see Table II), with a mixed-mode stress-based initiation law. After a critical cohesive stress value is reached, interfacial damage starts to evolve based on a mixed-mode damage evolution criterion (B-K criterion). The fracture toughness values were taken from mode-I and mode-II fracture tests and were held constant by adjusting the slope of the softening part of a classic traction-separation curve by using the characteristic length.

The thickness of the cohesive layers was equal to 5 percent of the nominal ply thickness. Thus, the fiber volume fraction was increased in the effective composite layers accordingly. Additionally, sectioning of scraps from the composite panels revealed a non-uniform distribution of fibers in the panels, yielding a higher fiber volume fraction near the gripped edges of the panel. This feature was incorporated into the FEAMAC model by utilizing a 67-percent fiber volume fraction in the gage section and a 70-percent fiber volume fraction near the gripped edges. Displacement boundary conditions were applied at one end of the specimen, and the other end was held fixed in the loading direction. Note, this introduces a nonhomogeneous stress state in the coupon, which can drive failure localization. This is significantly different than the micromechanics modeling strategy that homogenizes the entire coupon into the response of a single point, effectively treating the stresses in the coupon as uniform. Furthermore, boundary conditions along the specimen ends prohibited bending and twisting as well as rigid body movement during loading. The calibrated properties (Table II) were used in conjunction with the Plasticity-SE theory within FEAMAC to predict the failure response of the unnotched multidirectional laminates. Prediction results for both tension and compressive loading are presented in Figures 11 and 12. The experimentally reported stress-strain curve for Layups 1, 2, and 3 under tension were consistently underpredicted (with 20.2, 2.8, and 72.3 percent error, respectively) in ultimate strength, whereas the
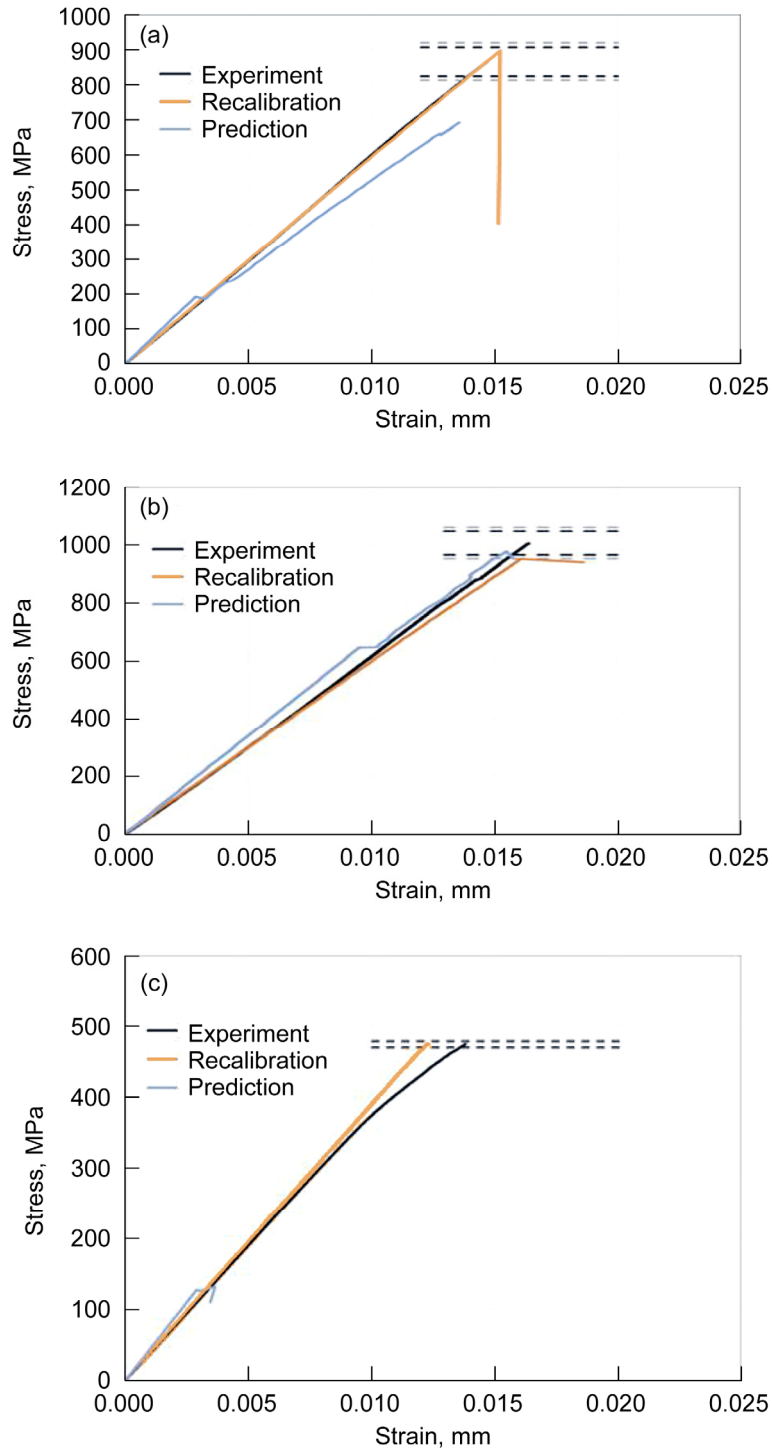
Figure 11.—Tension of unnotched IM7/977–3 carbon-fiber-reinforced epoxy composite laminates predicted and recalibrated using Plasticity-SE model within FEAMAC software. (a) Layup 1: [0,45,90, –45]$_{2S}$. (b) Layup 2: [0,60,0]$_{3S}$. (c) Layup 3: [30,60,90,–30,–60]$_{2S}$.
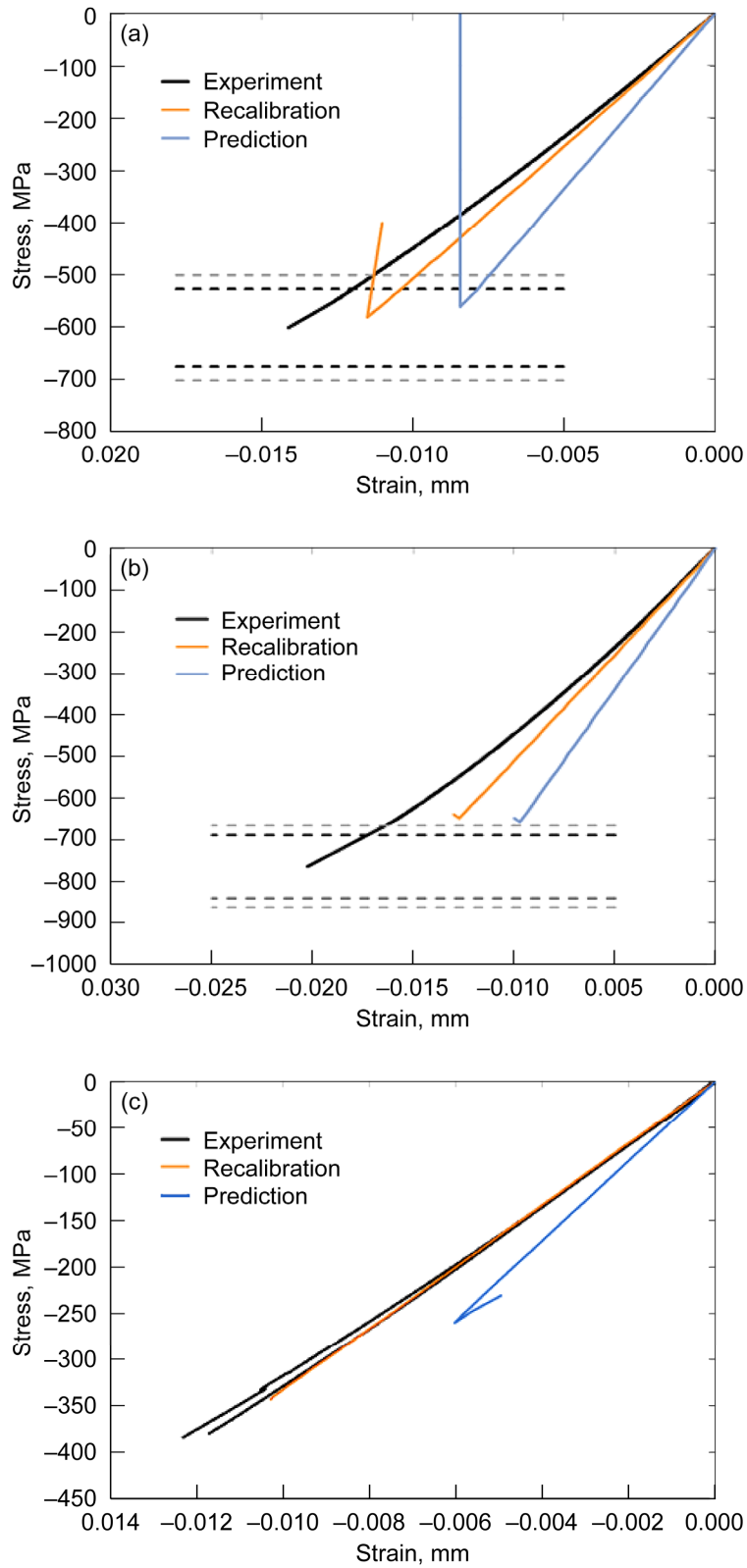
Figure 12.—Compression of unnotched IM7/977–3 carbon-fiber-reinforced epoxy composite laminates predicted and recalibrated using Plasticity-SE model within FEAMAC software. (a) Layup 1: [0,45,90, –45]$_{2s}$. (b) Layup 2: [0,60,0]$_{3s}$. (c) Layup 3: [30,60,90,–30,–60]$_{2s}$.

stiffness was overpredicted by approximately 11.9, 14, and 15.5 percent, respectively. Subsequent analysis revealed that the included matrix-rich layer and the cohesive elements were not the major source of the large difference observed in strength prediction for Layup 3. Potential sources of this error are going to be discussed further in Section 4.2.4. Similar to the predictions with MMCDM-SE, under compression the strength was consistently underpredicted, whereas the stiffness was always significantly overpredicted, because of the assumed low value for the 0° compression strength.

4.1.4 Recalibration (Plasticity-SE)

Similar to the MAC/GMC-MMCDM-SE recalibration, the fiber volume fraction of the RUC utilized within the gage section was set closer to the lower bound of the provided data (i.e., 62 percent) to improve FEAMAC-Plasticity-SE results. Additionally, the fiber's longitudinal modulus for tension was lowered to 256 GPa to match the ASTM standard recommendations for the computation of the composite's longitudinal stiffness (Ref. 11). Since a significantly lower compressive modulus was observed in the test data, the compressive modulus was also decreased to the same value used in the MMCDM-SE model (215 GPa). Also the compressive strength of the fiber was increased to match the recommended value in the literature (Ref. 11) (see Table IV). Most influential was the ultimate tensile matrix strain, which was increased almost fivefold to eliminate premature matrix failure. As shown in Section 4.2.4, this unrealistic modification is not necessary if the calibration process is done consistently. Modifications are shown in Table IV, and results are summarized in Figures 11 and 12. These changes significantly improved the results for each laminate whether loaded in tension or compression; that is, the stiffnesses are in better agreement with observation, and the predicted strengths of the unnotched test cases are still within the confidence bounds provided.

TABLE IV.—CONSTITUENT PROPERTIES AND INPUT PARAMETERS
USED TO RECALIBRATE PLASTICITY-SE MODEL FOR
IM7/977–3 CARBON FIBER/EPOXY LAMINATE

(a) Properties	(b) Parameters
Longitudinal modulus (fiber) E_{f11}^{T} = 256 GPa (tension)[a] E_{f11}^{C} = 215 GPa (compression)[a]	Ultimate fiber strain $\varepsilon_{f}^{T,\text{ult}}$ = 0.0161 (tension) $\varepsilon_{f}^{C,\text{ult}}$ = 0.0129 (compression)[a]
Transverse modulus (fiber) E_{f22} = 15 GPa	Fiber volume fraction V_f = 62 percent[a]
Longitudinal Poisson's ratio (fiber) ν_{f12} = 0.28	Ultimate matrix strain $\varepsilon_{m}^{\text{ult}}$ = 0.05[a]
Transverse Poisson's ratio (fiber) ν_{f23} = 0.19	Ultimate shear strain γ_{m}^{ult} = 0.06
Shear modulus (fiber) G_{f12} = 15 GPa	Interlaminar normal and shear stress $\tau_1 = \tau_2$ = 44 MPa
Young's modulus (matrix) E_m = 3.2 GPa	Strain energy release rate (tension) G_{I}^{c} ~ 0.25 mJ/mm² (mode I) G_{II}^{c} ~ 0.75 mJ/mm² (mode II)
Poisson's ratio (matrix) ν_m = 0.38	

[a]Entry was changed for recalibration.

4.1.5 Summary of Unnotched Analyses

The summary of static failure predictions and recalibrations for three different unnotched multidirectional layups utilizing the MMCDM-SE theory within MAC/GMC (microscale) and Plasticity-SE within FEAMAC (multiscale) is given in Table V. Briefly looking at the results, we can see that both methods demonstrated capability in reasonably predicting the tensile stiffness of all three layups with a maximum of 15.5 percent error, which was improved to 6 percent error during recalibration. The relative errors for tensile strength predictions varied from approximately 2 percent (for Layup 2) to 72 percent (for Layup 3), and were similarly greatly improved for Layups 1 and 3 during recalibration. A similar trend was observed for the strain-to-failure predictions as well. Note that because of the nonlinear nature of the stress-strain response, the percentage errors in strength and strain to failure are not necessarily the same. To claim that the response of the composite has been truly predicted, both stress and strain to failure must be accurate. For compression the maximum observed error in stiffness prediction was higher than in tension (40.4 percent for Layup 1), because of initial assumptions of compressive stiffness and ultimate strain values. During recalibration, significant improvements were made for all layups under compression as well.

TABLE V.—STIFFNESS, STRENGTH, AND MAXIMUM STRAIN DATA OF THREE DIFFERENT
UNNOTCHED CARBON/EPOXY IM7/977–3 COMPOSITE LAYUPS.
[Shaded column is experimental data; remaining columns are simulation results using
MMCDM-SE model within MAC/GMC and Plasticity-SE model within FEAMAC.]

(a) Stiffness, E

Layup[a,b]	E, GPa	Prediction[c]		Recalibration[c]	
		Plasticity-SE	MMCDM-SE	Plasticity-SE	MMCDM-SE
1 (T)	60.5	67.7 (11.91%)	67.5 (11.53%)	59.6 (−1.47%)	63.2 (4.45%)
2 (T)	59.5	67.8 (13.97%)	67.5 (13.37%)	59.7 (0.32%)	63.2 (6.17%)
3 (T)	38.0	43.9 (15.50%)	42.0 (10.36%)	38.9 (2.24%)	39.5 (3.76%)
1 (C)	48.0	67.4 (40.48%)	54.3 (13.24%)	50.9 (6.13%)	50.3 (4.79%)
2 (C)	48.9	67.8 (38.74%)	54.3 (11.14%)	51.2 (4.77%)	50.3 (2.84%)
3 (C)	33.5	42.9 (28.07%)	34.5 (3.07%)	33.3 (−0.55%)	34.5 (3.02%)

(b) Maximum strength, σ_{max}

Layup[a,b]	σ_{max}, MPa	Prediction[c,d]		Recalibration[c,e]	
		Plasticity-SE	MMCDM-SE	Plasticity-SE	MMCDM-SE
1 (T)	866	691 (−20.2%)	1033 (19.25%)	897.0 (3.58%)	957 (10.46%)
2 (T)	1005	977 (−2.82%)	1025 (1.99%)	951.0 (−5.40%)	954 (−5.13%)
3 (T)	473	131 (−72.3%)	789 (66.76%)	474.0 (0.18%)	471 (−0.41%)
1 (C)	603	562.0 (−6.8%)	483 (−19.95%)	584.0 (−3.15%)	621 (3.00%)
2 (C)	765	659.0 (−13.9%)	483 (−36.97%)	649.0 (−15.2%)	711 (−7.16%)
3 (C)	382	260.0 (−31.9%)	446 (16.76%)	351.0 (−8.12%)	398 (4.22%)

(c) Maximum strain, ε_{max}

Layup[a,b]	ε_{max}	Prediction[c,d]		Recalibration[c,e]	
		Plasticity-SE	MMCDM-SE	Plasticity-SE	MMCDM-SE
1 (T)	0.014	0.013 (−7.1%)	0.017 (21.4%)	0.015 (7.1%)	0.017 (21.4%)
2 (T)	0.015	0.015 (0.1%)	0.017 (13.3%)	0.016 (6.6%)	0.016 (13.3%)
3 (T)	0.013	0.003 (−76.9%)	0.022 (69.2%)	0.012 (−7.6%)	0.013 (0.1%)
1 (C)	0.014	0.008 (−42.8%)	0.009 (−35.7%)	0.012 (−14.2%)	0.014 (0.1%)
2 (C)	0.021	0.009 (−57.1%)	0.009 (−57.1%)	0.012 (−42.8%)	0.017 (−19%)
3 (C)	0.012	0.007 (−41.6%)	0.013 (8.3%)	0.011 (−8.3%)	0.012 (0.1%)

[a]Layup 1: [0,45,90,–45]$_{2S}$; Layup 2: [+60,0,–60]3S; and Layup 3: [+30,+60,90,–60,–30]$_{2S}$.
[b]T is tension and C is compression.
[c]Quantities in parentheses represent error.

In reality, localization within unnotched composite layups occurs from variations in residual stress and preexisting flaws (resulting from manufacturing and processing) in the material. However, it is very difficult to characterize these flaws and/or residual stress fields. As such, modeling coupon laminates with FEM by including initial flaws or utilizing other localization strategies is a challenging task and often leads to inherent mesh dependence within a multiscale framework (Refs. 15 to 17). Moreover, pathological mesh dependence is well known to occur in any numerical solution where there is strain softening (i.e., negative tangent stiffness), and no attempt is made to regularize the dissipated energy (Refs. 18 to 20). Additionally, when the SE method is also utilized for the fibers in standalone MAC/GMC, there is no length scale dependence because there is no finite dimensionality associated with the x_1-direction (Fig. 1) in the doubly-periodic formulation of GMC (idealized to be infinitely long). Conversely, once GMC is embedded within the FEM, via FEAMAC, a finite length is immediately linked to the x_1-direction at the microscale (i.e., it is equal to element size). Consequently, the SE method for the fiber also becomes pathologically mesh dependent. Various mesh-objective solutions together with a micromechanical localization strategy would alleviate this inherent mesh dependency (Refs. 15 to 20). The consequence of such localization factors and strategies (utilized for predicting the strength of coupons) will be investigated in future studies.

4.2   Notched Laminate

A notched laminate has a geometry that induces stress-strain gradients and thus point-to-point interaction within the continuum that cannot be modeled with MAC/GMC alone. Therefore, the FEAMAC multiscale framework was utilized, in conjunction with plastic theory and the SE method together with the in-built delamination model in the FE software Abaqus, to model the response of the three-notched laminate coupons (Layup 1: $[0,45,90,-45]_{2S}$, Layup 2: $[+60,0,-60]_{3S}$, and Layup 3: $[+30,+60,90,-60,-30]_{2S}$). The same element types and modeling strategies, described in Sections 4.1.3 and 4.1.4 for unnotched laminates, were employed for notched laminates, except now uniform fiber volume fraction is used throughout the coupons since the presence of the notch localizes natural stress-riser-driving strain upon failure. Figure 13 shows different meshes (the tensile specimen is 138 mm long, whereas the compression specimen is 250 mm long, but both have the same width) used to analyze this layup under tension and compression (tabs are excluded).
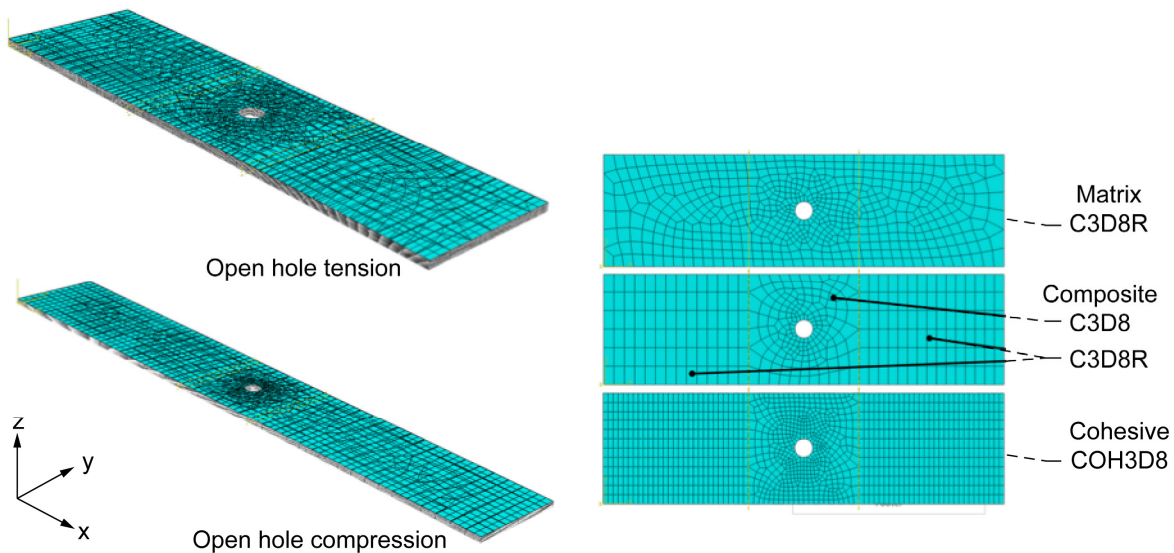
Figure 13.—Plasticity-SE finite element meshes to be used in FEAMAC to analyze all three layups of notched IM7/977–3 carbon-fiber-reinforced epoxy composite laminate.

4.2.1 FEAMAC Prediction: Plasticity-SE

Using the aforementioned FE model description, the constituent properties calibrated for the Plasticity-SE theory (Table II) were used in conjunction with FEAMAC to predict the failure response of the notched multidirectional laminate specimens. The blind predictions (stress-strain curves) for these layups are compared with reported experiments in Figures 14 and 15. The tensile stiffness prediction matched the experimental result very well with less than 5 percent error for all layups. However, the tensile strength was underpredicted by 20.3, 26.3, and 72.3 percent for Layups 1, 2, and 3, respectively. Similar to the unnotched laminates, compressive stiffness is consistently overpredicted and compressive strength is underpredicted because of the initially assumed high compressive fiber modulus and low compressive fiber strength.
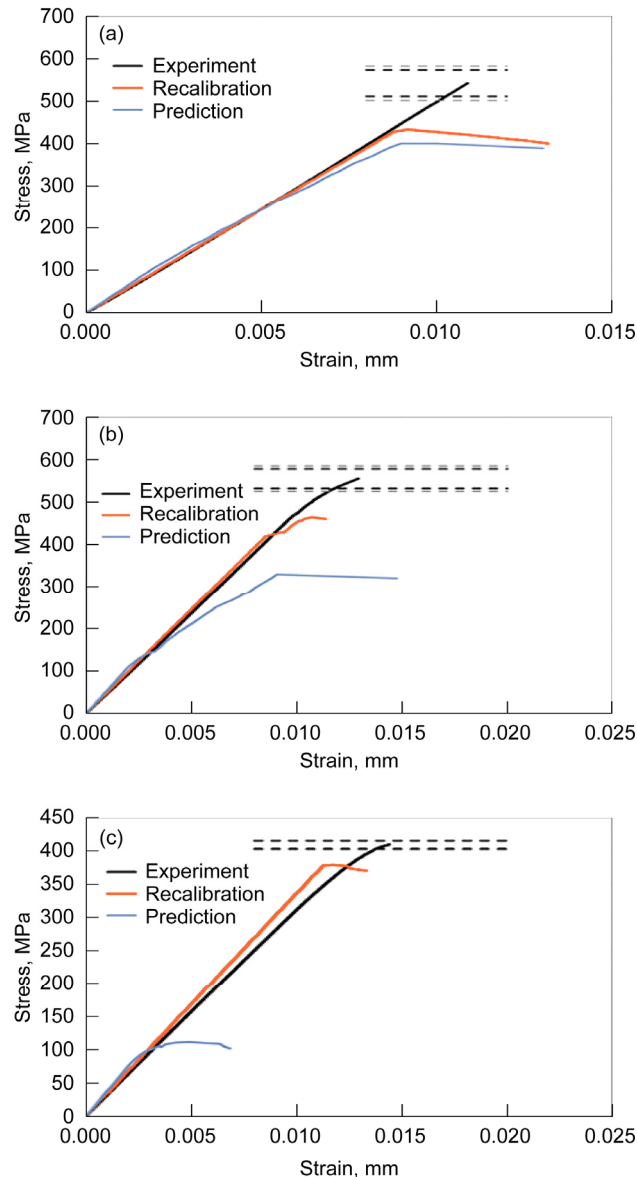
Figure 14.—Tension of notched IM7/977–3 carbon-fiber-reinforced epoxy composite laminates predicted and recalibrated using Plasticity-SE model within FEAMAC software. (a) Layup 1: $[0,45,90,–45]_{2s}$. (b) Layup 2: $[0,60,0]_{3s}$. (c) Layup 3: $[30,60,90,–30,–60]_{2s}$.
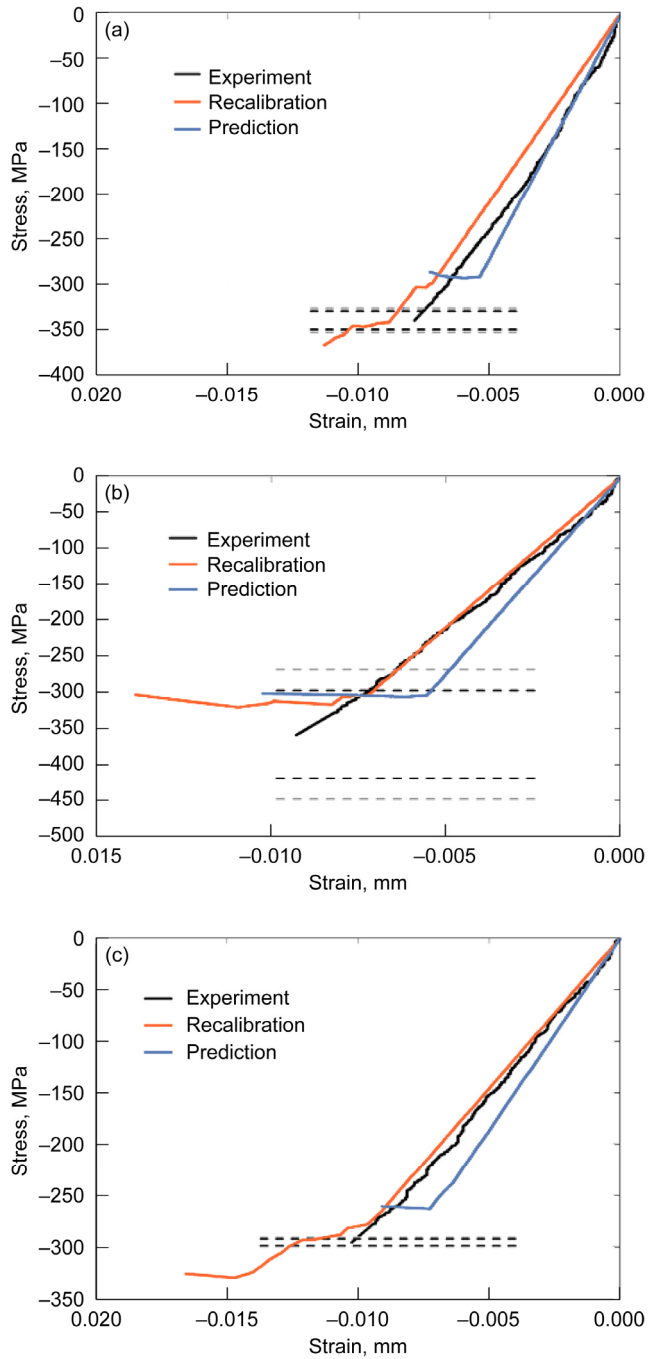
Figure 15.—Compression of notched IM7/977–3 carbon-fiber-reinforced epoxy composite laminates predicted and recalibrated using Plasticity-SE model within FEAMAC software. (a) Layup 1: [0,45,90,–45]$_{2S}$. (b) Layup 2: [0,60,0]$_{3S}$. (c) Layup 3: [30,60,90,–30,–60]$_{2S}$.

4.2.2   FEAMAC Recalibration: Plasticity-SE

The same recalibrated properties obtained from the unnotched laminates modeled with Plasticity-SE (Section 4.1.4, Table IV) were used for the recalibration phase corresponding to the notched laminates. Results are shown in Figures 14 and 15. With the applied modifications the tensile strength predictions were significantly improved, particularly for Layups 2 and 3; however, all simulated strength values are still lower than the given experimental confidence bounds. Similarly, the compressive stiffness and strength predictions were greatly improved and showed very good agreement, compared with experimental results.

Figure 16 shows contour plots of equivalent inelastic strain (an available measure of damage) for individual plies of Layups 1 to 3 at 90 percent failure. X-ray plots provided by AFRL for each ply are also provided for easy comparison of simulation with measured damage states. The damage measured around the notch shows a progressive outward growth pattern for all layups, with damage initiating first in the 90° layer. It must be noted, however, that this equivalent plastic strain is not an adequate measure of damage as it does not consider fracture modes, which are clearly visible in the x-rays. Furthermore, in the present case the equivalent plastic strain is smeared over the composite RUC, and thus cannot resolve local failure modes such as matrix cracking.

4.2.3   Summary of Notched Analyses

The summary of the multiscale static failure predictions and recalibrations for the three different notched multidirectional layups utilizing Plasticity-SE within FEAMAC are given in Table VI. One can readily see that in the case of tension FEAMAC-Plasticity-SE predictions were in good agreement with the measured tensile stiffness for all three layups with a maximum of 5 percent error, which was improved to less than 4 percent error during recalibration. Because of the nonlinear composite behavior, the percentage error in strain-to-failure does not directly correlate with the ultimate strength. Once the compressive strength and modulus of the fiber were adjusted, significant improvements were observed in compressive stiffness and strength predictions for all three layups.

4.2.4   Notched Laminates: 3D to 2D Idealization—FEAMAC

In order to better understand the effect of element dimensionality (or idealization consistency) on the obtained FEAMAC solution, the 3D notched mesh used within this study was reduced to a 2D composite shell mesh (S4R) with the exact same mesh density, boundary conditions, and constituent properties (listed in Table II). This plane-stress solution is significantly more consistent with the plane-stress lamination formulation employed within MAC/GMC utilized during the characterization phase, wherein the in situ fiber/matrix constituent material model parameters were obtained given simple [0], [90], and [±45] unnotched laminate behavior (see Sec. 3.0). Utilization of this 2D composite mesh instead of the prior 3D mesh resulted in consistent improvement in blind strength predictions for all three layups, wherein the prediction error was reduced to less than 6 percent for all layups (Figs. 17 and 18). The improvement in tensile strength predictions using a 2D versus 3D mesh was generally greater than when the laminates were subjected to compression, with the most significant difference observed in Layup 3 under tension (Fig. 17(c)). A similar trend was observed for unnotched specimens as well. A summary of static failure prediction parameters (i.e., stiffness, ultimate stress, and ultimate strain) for the three different notched multidirectional layups utilizing a 2D mesh and FEAMAC-Plasticity-SE are given in Table VII.
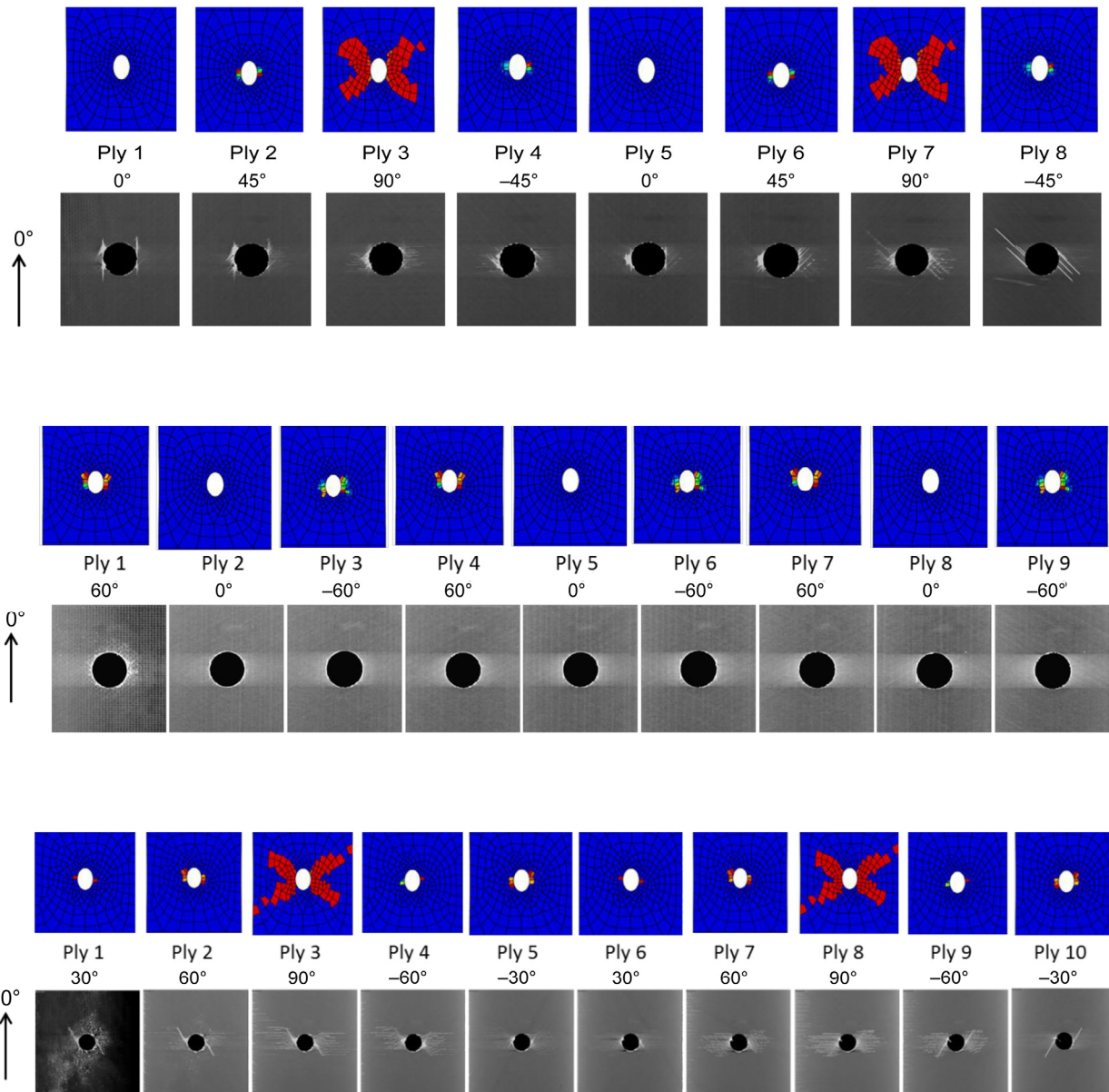
Figure 16.—Inelastic strain contour plots using Plasticity-SE model within FEAMAC software and x-ray images of individual plies for notched IM7/977–3 carbon-fiber-reinforced epoxy composite laminate.

TABLE VI.—STIFFNESS, STRENGTH, AND MAXIMUM
STRAIN DATA OF THREE DIFFERENT UNNOTCHED
CARBON/EPOXY IM7/977–3 COMPOSITE LAYUPS
[Shaded column is experimental data; remaining columns
are simulation results using Plasticity-SE model within
FEAMAC.]

(a) Stiffness, E

Layup[a,b]	E, GPa	Plasticity-SE prediction[c]	FEAMAC recalibration[c]
1 (T)	48.3	46.7 (3.3%)	49.1 (1.6%)
2 (T)	48.8	51.1 (4.7%)	48.9 (0.2%)
3 (T)	32.4	33.5 (3.3%)	33.6 (3.7%)
1 (C)	44.5	54.3 (22%)	41.6 (−6.5%)
2 (C)	44.4	54.8 (23%)	41.9 (−5.6%)
3 (C)	30.1	37.4 (25%)	29.1 (−3.3%)

(b) Maximum strength, σ_{max}

Layup[a,b]	σ_{max}, MPa	Plasticity-SE prediction[c]	FEAMAC recalibration[c]
1 (T)	554	329 (−40.6%)	464 (−16.2%)
2 (T)	543	400 (−26.3%)	433 (20%)
3 (T)	409	111 (−72.8%)	378 (−7.5%)
1 (C)	341	294 (−13.7%)	367 (7.6%)
2 (C)	358	305 (−14.8%)	320 (−10.6%)
3 (C)	295	263 (−11.0%)	329 (11.5%)

(c) Maximum strain, ε_{max}

Layup[a,b]	ε_{max}	Plasticity-SE prediction[c]	FEAMAC recalibration[c]
1 (T)	0.0125	0.011 (−12%)	0.01 (−20%)
2 (T)	0.011	0.008 (−27%)	0.008 (−27%)
3 (T)	0.014	0.006 (−57%)	0.012 (−14%)
1 (C)	0.0075	0.004 (−46%)	0.008 (−6%)
2 (C)	0.009	0.006 (−33%)	0.008 (−11%)
3 (C)	0.01	0.007 (−30%)	0.011 (−10%)

[a]Layup 1: $[0,45,90,-45]_{2S}$; Layup 2: $[+60,0,-60]_{3S}$; and
Layup 3: $[+30,+60,90,-60,-30]_{2S}$.
[b]T is tension and C is compression.
[c]Quantities in parentheses represent error.
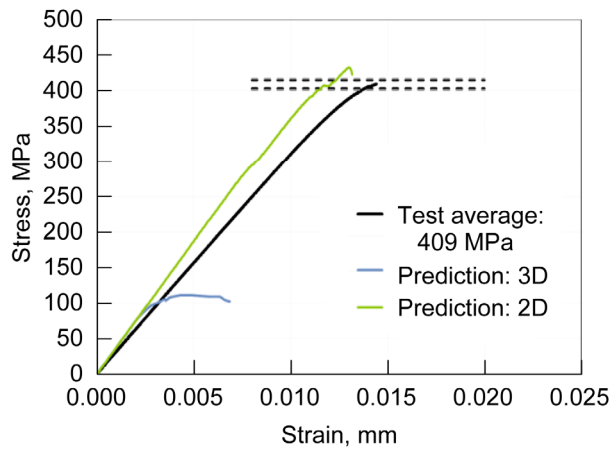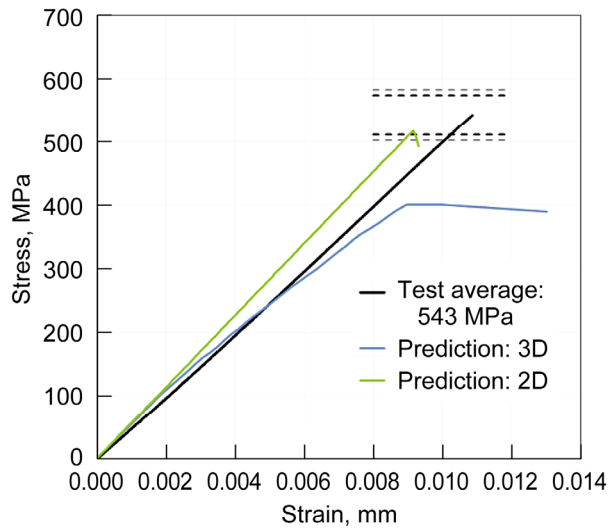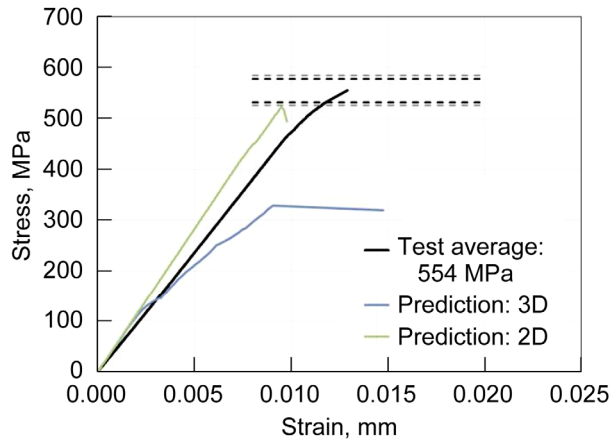
Figure 17.—Comparison of two- versus three-dimensional mesh in prediction of tension in notched IM7/977–3 carbon-fiber-reinforced epoxy composite laminates using Plasticity-SE model within FEAMAC software. (a) Layup 1: [0,45,90,–45]$_{2S.}$ (b) Layup 2: [0,60,0]$_{3S.}$ (c) Layup 3: [30,60,90,–30,–60]$_{2S.}$
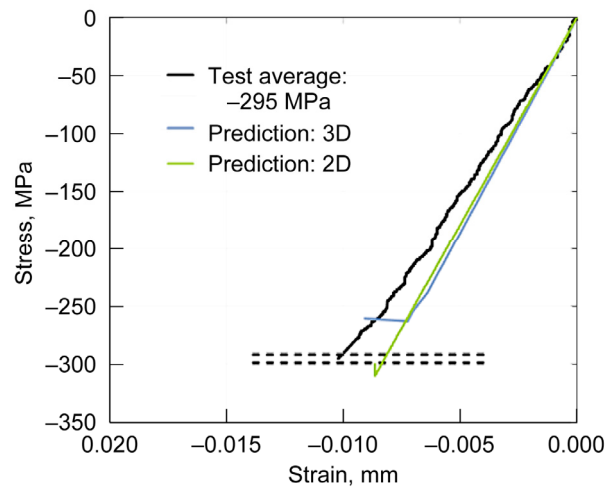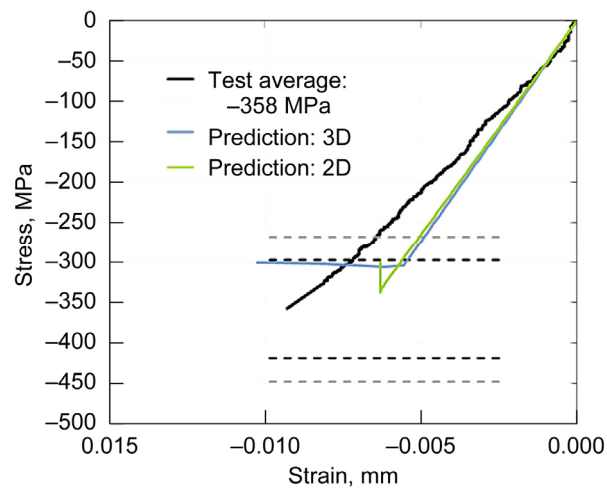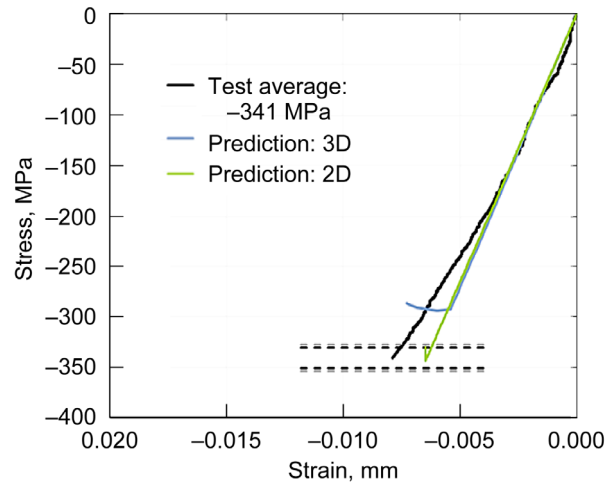
Figure 18.—Comparison of two- versus three-dimensional
mesh in prediction of compression in notched IM7/977–3
carbon-fiber-reinforced epoxy composite laminates using
Plasticity-SE model within FEAMAC software. (a) Layup 1:
$[0,45,90,-45]_{2S}$. (b) Layup 2: $[0,60,0]_{3S}$. (c) Layup 3:
$[30,60,90,-30,-60]_{2S}$.

TABLE VII.—STIFFNESS, STRENGTH, AND MAXIMUM STRAIN DATA FOR THREE
DIFFERENT NOTCHED CARBON/EPOXY IM7/977–3 COMPOSITE LAYUPS IN
TWO-DIMENSIONAL SIMULATION

[Shaded columns are experimental data; remaining columns are simulation results using
two-dimensional mesh and Plasticity-SE model within FEAMAC.]

Layup[a,b]	Stiffness, E, GPa	FEAMAC prediction[c]	Maximum strength, σ_{max}, GPa	FEAMAC prediction[c]	Maximum strain, ε_{max}	FEAMAC prediction[c]
1 (T)	48.3	46.7 (3.3%)	554	522 (5.7%)	0.0125	0.01 (–20%)
2 (T)	48.8	51.1 (4.7%)	543	529 (2.6%)	0.011	0.008 (–27%)
3 (T)	32.4	33.5 (3.3%)	409	428 (4.6%)	0.014	0.012 (–14%)
1 (C)	44.5	54.3 (22%)	341	342 (0.3%)	0.0075	0.006 (20%)
2 (C)	44.4	54.8 (23%)	358	343 (4.1%)	0.009	0.007 (22%)
3 (C)	30.1	37.4 (25%)	295	315 (6.7%)	0.01	0.0085 (15%)

[a]Layup 1: [0,45,90,–45]₂s; Layup 2: [+60,0,–60]₃s; and Layup 3: [+30,+60,90,–60,–30]₂s.

[b]T is tension and C is compression.

[c]Quantities in parentheses represent error.

The available literature data focusing on the differences between 2D and 3D nonlinear FE analysis are unfortunately very sparse (Refs. 14, 21, and 22). Similarly, as far as the authors know, no large-scale systematic studies focusing on differences between 2D and 3D multiscale analyses have been reported in the literature. This section depicts initial observations regarding dimensional consistency; a more in-depth systematic 2D and 3D element multiscale analysis study is planned in the near future. The observed difference in predicted strength between 2D and 3D results in Layup 1 and Layup 2 lies in the reported range of variation by Krueger et al. (Ref. 21) and Yao and Qu (Ref. 22) for single-scale analysis. However, the difference in Layup 3 is much higher than the other two layups, especially under tension. These preliminary results illustrate the importance of preserving idealization consistency (i.e., model dimensionality) from characterization to prediction—particularly when conducting multiscale analysis, since damage evolution at the local level is highly influenced by the applied stress-strain state on the RUC. The significance of this consistency appears to be highly dependent upon the specific constituent deformation or damage models being utilized within the micromechanics analysis (i.e., RUC); for example, Plasticity-SE was significantly more influenced than was MMCDM-SE. Note if one utilizes a macromechanics analysis framework (one in which the composite behavior is idealized by an anisotropic constitutive model), this need for consistency is hardly perceptible. The importance of this consistency was further confirmed by utilizing the constituent model parameters obtained from the 3D recalibration phase within the 2D analysis and shown to significantly overpredict experimental results. It is conjectured that the extremely high difference observed in predicted strength values for Layup 3 (or any other layup without [0] plies) may stem from (1) deficiencies in the micromechanical model, (2) the deviatoric J2 assumption associated with Plasticity-SE, (3) the multiscale framework, or (4) a combination of these factors. All these factors will be studied extensively in the near future utilizing the present results as a baseline.

4.2.5 Stochastic Fiber Failure Model to Alleviate Mesh Dependence

Despite longer computational times, a uniform fine mesh is necessary in many types of highly localized nonlinear analyses in order to ensure a sufficiently accurate prediction of the stress state in the gage section of a notched specimen. Moreover, a preliminary mesh sensitivity study revealed the maximum mesh size around the notch must be smaller than 1.3 mm to ensure convergence or saturation of the global elastic stress state. Accordingly, a uniform 2D fine mesh, with element size of 1 mm², was employed. The results (see Figs. 19 and 20, line labeled "Mesh-2D-fine (1 mm)") are compared to the previously coarser 2D mesh, results labeled "Mesh-2D-coarse."
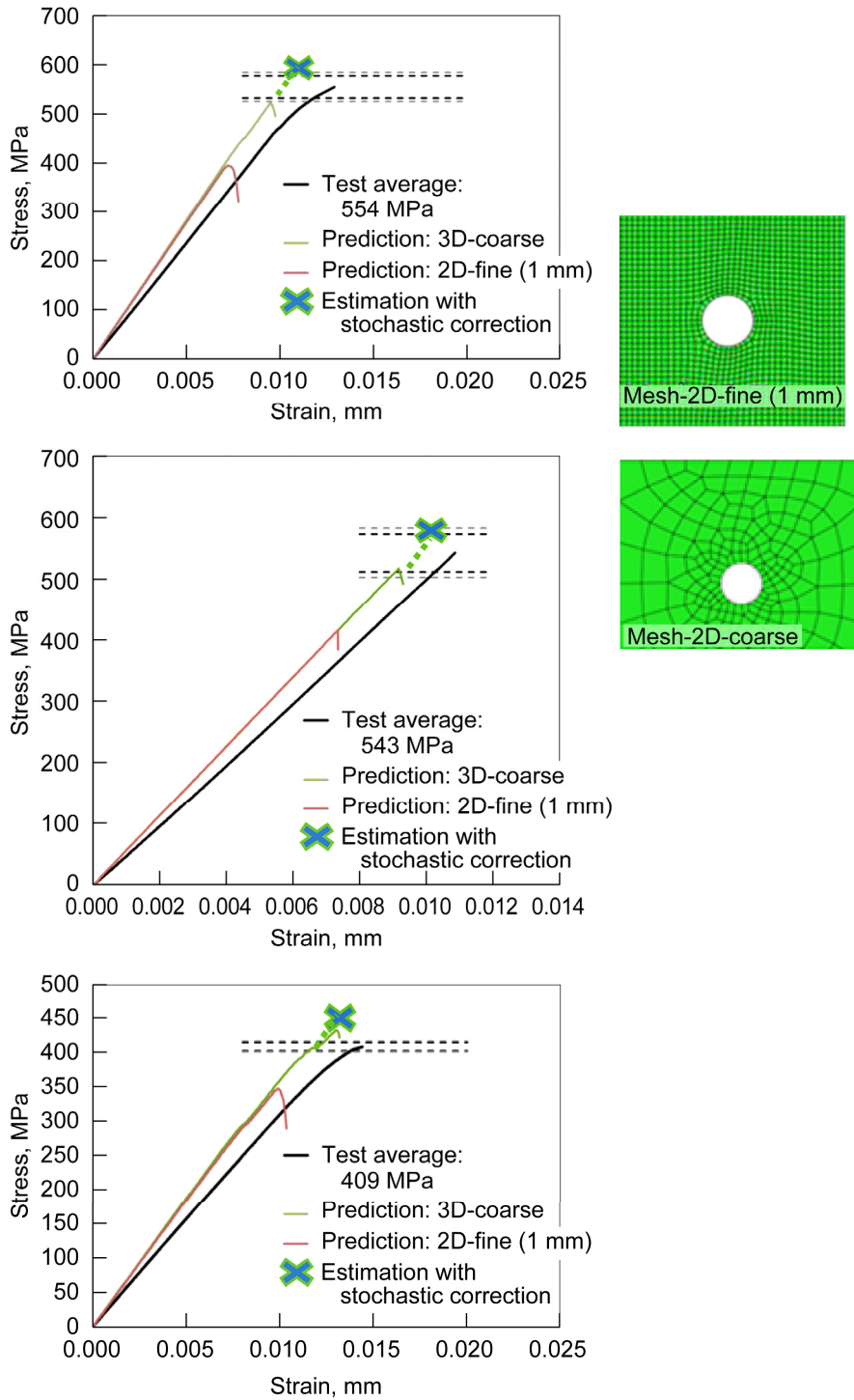
Figure 19.—Comparison of coarse versus fine mesh in prediction of tension in notched IM7/977–3 carbon-fiber-reinforced epoxy composite laminates using Plasticity-SE model within FEAMAC software. (a) Layup 1: $[0,45,90,-45]_{2S}$. (b) Layup 2: $[0,60,0]_{3S}$. (c) Layup 3: $[30,60,90,-30,-60]_{2S}$.
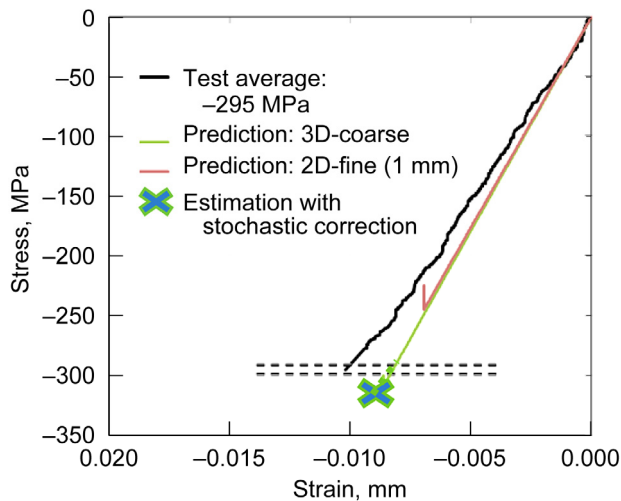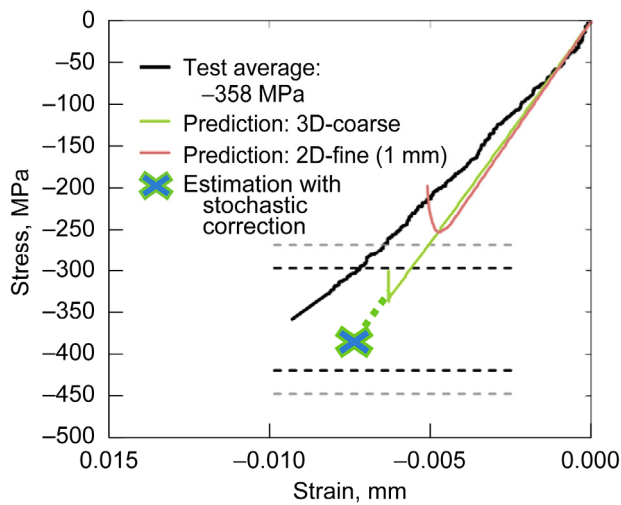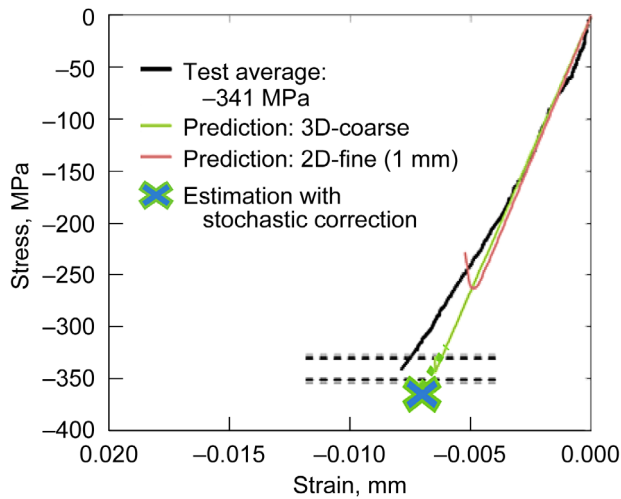
Figure 20.—Comparison of using coarse versus fine mesh in prediction of compression in notched IM7/977–3 carbon-fiber-reinforced epoxy composite laminates using Plasticity-SE model within FEAMAC software. (a) Layup 1: [0,45,90,–45]$_{2S}$. (b) Layup 2: [0,60,0]$_{3S}$. (c) Layup 3: [30,60,90,–30,–60]$_{2S}$.

As observed from the results in Figures 19 and 20, the FEAMAC-Plasticity-SE results for static strength (note the effective stiffness is unaffected by mesh size, as expected) are highly mesh dependent because the degradation scheme leads to element-volume-dependent energy dissipation (Refs. 18 to 20). Since carbon fiber strength is known to be highly volume sensitive (Refs. 23 and 24), the effective longitudinal failure stress associated with the fiber will be significantly influenced by the volume of the material within a given FE mesh. Therefore, the relative damage length scale associated with a given FE analysis as compared with that length scale used for characterization must be accounted for to decrease this pathological FE volume dependence. Utilizing the well-known Weibull volume fraction equation (Ref. 25) allows manual adjustment of the carbon fiber strength for a given FE volume (i.e., mesh density):

$$\frac{\sigma_2}{\sigma_1} = \left(\frac{A_1}{A_2}\right)^{1/m} \tag{8}$$

A_1 is the original area assumed for characterization (i.e., the entire gage area of the specimen, 25 by 12.5 mm in the current study), and A_2 is the area associated with the size of the FE used in the notched laminate analysis (i.e., 1 mm^2); σ_1, and σ_2 are their corresponding stress values. Given the observed scatter in the unidirectional $[0]_8$ characterization experiments (sample size involved 8 specimens) conducted by AFRL and assuming a confidence interval of 95 percent ($[0]_8$: 12 to 38.5 MPa, Layup 1: 13.8 to 62 MPa, and Layup 2: 17 to 74 MPa), a reasonable Weibull parameter, m, of the carbon fiber static strength was determined to be approximately 16 (see Fig. 21). If the bias correction factor having only 5 or 6 data points is taken into account, this m could be arguably as low as 13.5.
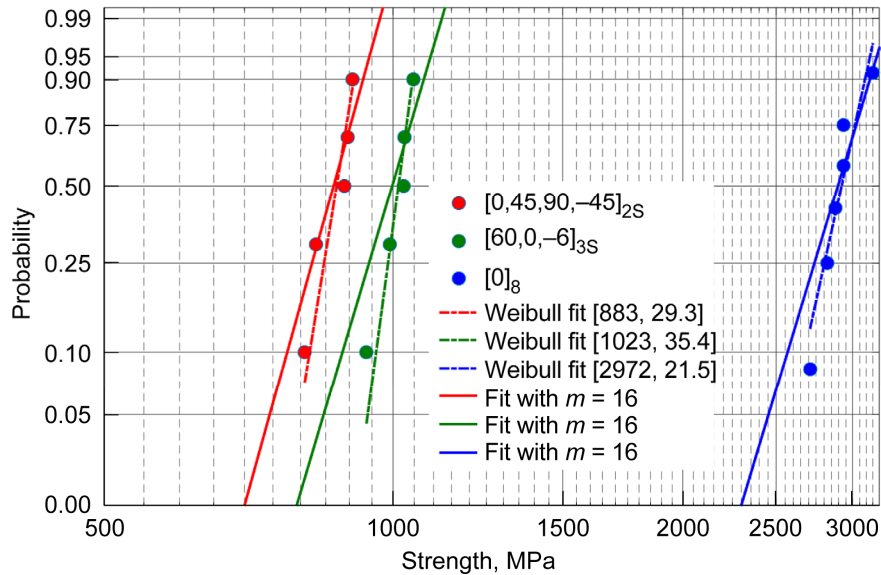
Figure 21.—Weibull distribution (with Weibull parameter, m) and data scatter in experiments conducted by the Air Force Research Laboratory.

Unfortunately, applying the above-mentioned volume correction method for the original non-uniform coarse 2D mesh (i.e., Mesh-2D-coarse) is a complex task because of varying element area throughout the gage section. Consequently, for expediency an average weighted area of the elements within the gage section (9.51 mm^2) gives a rough estimate of 24 percent strength enhancement that would be achieved through the volume correction method for this non-uniform coarse mesh. Had this enhancement been applied, the obtained strength levels would be mostly within reported margins for both tension and compression (see the X symbols in Figs. 19 and 20). When the carbon fiber strength is enhanced by using the above-stated Equation (8) for the new fine mesh (Mesh-2D-fine, (1 mm)), a much better agreement is achieved between numerical and experimental results (Figs. 22 and 23). This is further approved by applying the same enhancement methodology to a finer (Mesh-2D (0.7 mm)) and a coarser mesh (Mesh-2D (1.3 mm)). It is observed from Figure 22 (Layups 1 and 2) and Figure 23 (Layups 1 and 2), the pathological mesh dependence in FEAMAC-Plasticity-SE can be addressed reasonably well by the volume correction method, particularly in fiber dominated laminates (Layups 1 and 2), where final failure is primarily governed by 0° ply strength, as compared to Layup 3, which does not contain 0° plies. Therefore, this method can be considered a useful tool for improvement of the inherent strength dependence on volume and should be employed to partially (but not completely) alleviate the pathological mesh dependence of fiber-dominated layups for a given FE analysis. Other strength-scaling techniques have been demonstrated in the literature (see Refs. 26 and 27). Note the recalibration results in Figures 22 and 23 include minor modifications of the fiber stiffness under tension and compression (as discussed previously in the recalibration section, Sec. 4.2.2) in addition to the Weibull volume adjustment. Clearly, the numerical results match the experiments with minimal error for all three layups under both tension and compression loading.
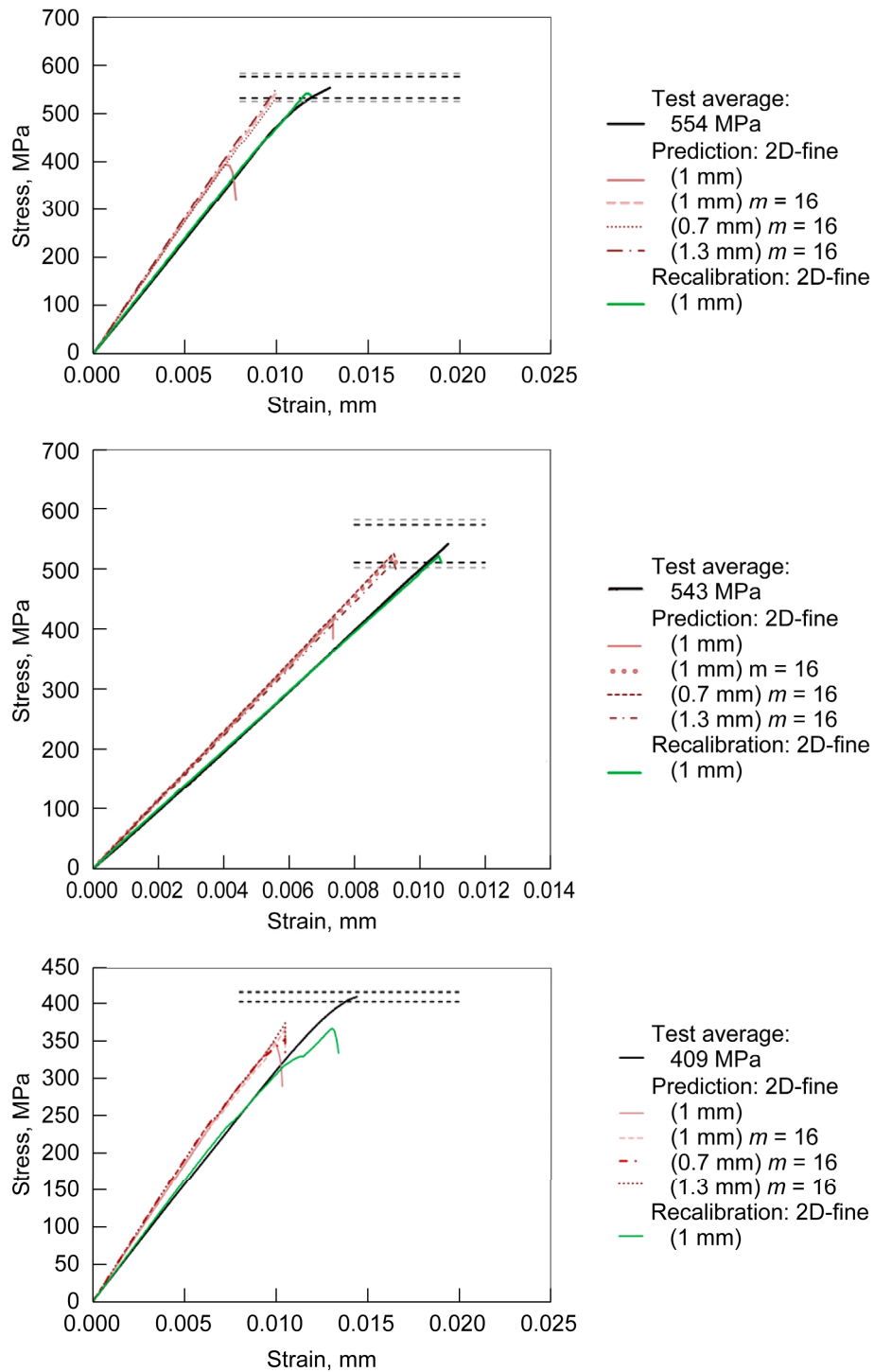
Figure 22.—Tension of notched IM7/977–3 carbon-fiber-reinforced epoxy composite laminates predicted and recalibrated using Plasticity-SE model within FEAMAC software; comparison of using different element sizes of 0.7, 1, and 1.3 mm (with Weibull parameter, m). (a) Layup 1: $[0,45,90,-45]_{2s}$ (b) Layup 2: $[0,60,0]_{3s}$. (c) Layup 3: $[30,60,90,-30,-60]_{2s}$.
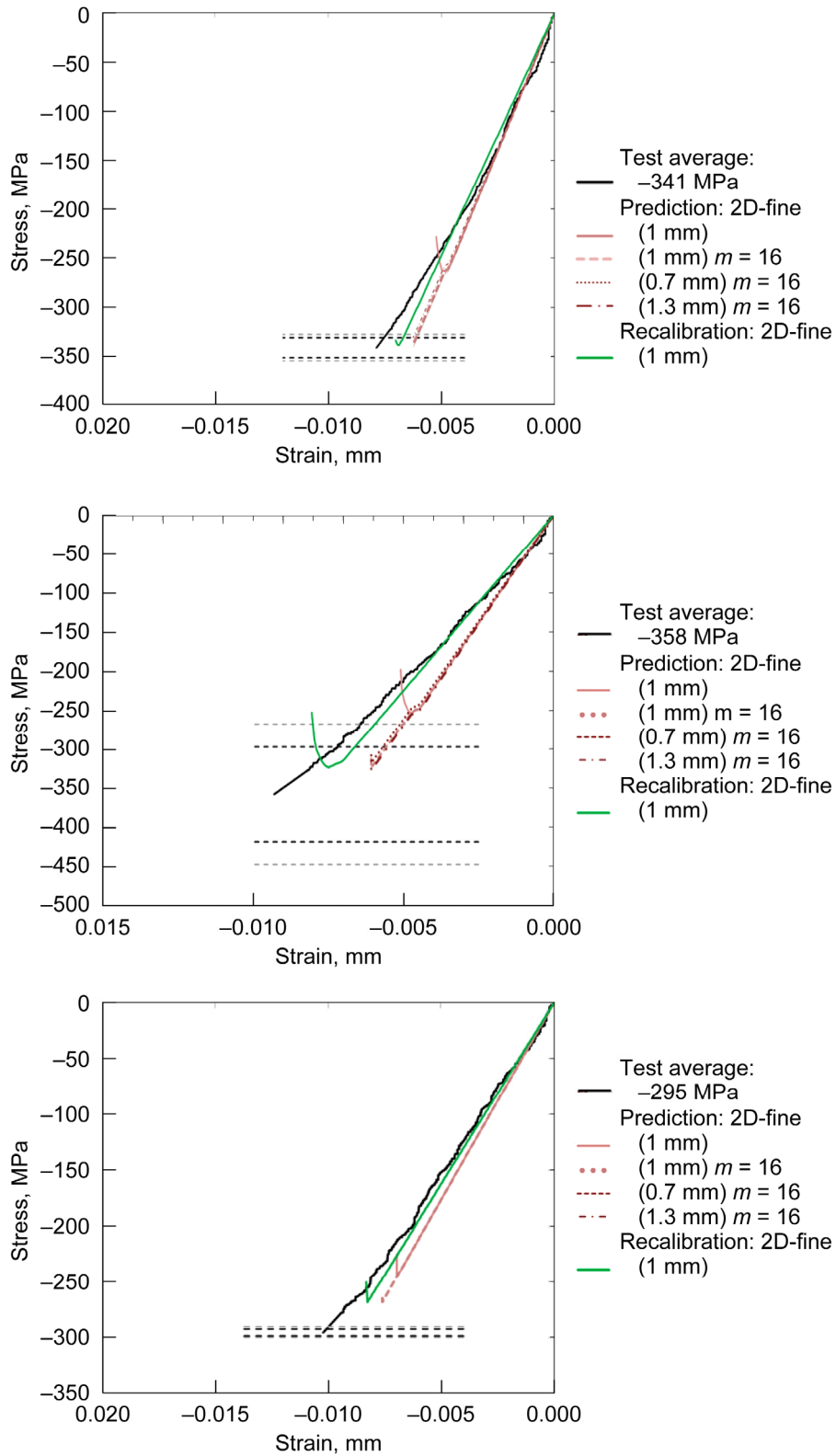
Figure 23.—Compression of notched IM7/977–3 carbon-fiber-reinforced epoxy composite laminates predicted and recalibrated using Plasticity-SE model within FEAMAC software; comparison of using different element sizes of 0.7, 1, and 1.3 mm (with Weibull parameter, m). (a) Layup 1: $[0,45,90,-45]_{2s}$. (b) Layup 2: $[0,60,0]_{3s}$. (c) Layup 3: $[30,60,90,-30,-60]_{2s}$.

5.0 Conclusion

Herein, a micromechanics-based multiscale analysis of the monotonic static tensile and compressive behavior of three carbon/epoxy (IM7/977–3), unnotched and notched multidirectional layups (Layup 1: $[0,45,90,-45]_{2S}$, Layup 2: $[0,60,0]_{3S}$, and Layup 3: $[30,60,90,-30,-60]_{2S}$) was conducted. The tools utilized were the MAC/GMC (Micromechanics Analysis Code with Generalized Method of Cells, which analyzes response at a material point) and FEAMAC (which is the multiscale implementation of MAC/GMC within the FEM) developed at the NASA Glenn Research Center. Matrix nonlinearity was modeled in two ways: progressive damage and plasticity. Results of this study have demonstrated that both MAC/GMC and FEAMAC are viable tools for the modeling of unnotched and notched laminates, respectively. The computational efficiency for MAC/GMC (run times on the order of seconds using one central processing unit (CPU) affords designers the opportunity to conduct thorough trade studies. Moreover, once the constituent parameters have been calibrated sufficiently, it appears (through this demonstration) that MAC/GMC provides the correct trends and holds predictive potential for unnotched laminates. When incorporation of structural features (such as notches or holes) is required, the FEAMAC multiscale framework must be utilized. The applicability of FEAMAC was similarly demonstrated herein for both unnotched and notched laminates, although at an added computational cost, depending upon the element type and number of elements for which micromechanics (multiscale) analysis is performed.

Specifically, it was shown:

Tensile loading

-Stiffness was slightly overpredicted for both notched and unnotched laminates.

-Ultimate strength for all three layups of the unnotched coupons was overpredicted using MAC/GMC-MMCDM-SE, whereas it was underpredicted with FEAMAC-Plasticity-SE.

Compressive loading

-Stiffness was overpredicted because of the assumed low value for the 0° compression strength.

-Strength and strain were consistently underpredicted for the unnotched coupons.

Observed discrepancies in the stress-strain response of the unnotched and notched laminates were significantly improved with only minor modifications to the model parameters in both models (MMCDM and plasticity).

Although based only on preliminary observations, a key lesson learned is the need to preserve model dimensionality (idealization consistency) throughout the characterization and prediction phase of any given analysis, when conducting multiscale (micromechanics based) analyses, if one wants to minimize inconsistencies arising from stress state variations in three- and two-dimensional (3D and 2D) elements. Also, because of high computational cost and restricted CPU power of FEAMAC (no more than a single CPU can be accessed), no mesh-sensitivity studies were conducted during the limited timeframe of this study. Clearly, refining the 3D mesh within the gage section in all directions (length, width, and thickness) would enhance accurately capturing the nonlinear in-plane and out-of-plane stress states and dominant failure mechanisms (e.g., delamination). Therefore, caution should be exercised in drawing conclusions based on the current 3D mesh density used in the current study relative to the underlying constituent models or micromechanics method employed. However, qualitative trends relative to predictive ability will most likely hold since the same mesh density was preserved throughout the whole study and most importantly when studying 3D-to-2D element conversions. The influence of mesh refinement was addressed in the 2D analysis with additional plans for future studies as well.

Finally, this exercise has revealed that, as multiscale models become more popular within the research community, a paradigm shift in test methods is required to facilitate their use in industry. The coupon-level experiments used in this study to characterize and calibrate the constituent-level constitutive models should actually serve as validation data for the micromechanics or multiscale models. In order to truly evaluate the predictive capability of microscale and multiscale models, constituent data (both deterministic and stochastic) must be provided and the coupon behavior be predicted. Unnotched, unidirectional coupon experiments do not provide all the necessary data needed to characterize

sophisticated progressive damage models. Without any precursor for failure localization, the failure of unnotched coupons depends on subscale inhomogeneities, which cannot be characterized with the requisite accuracy needed for reliable prediction of failure. Furthermore, unidirectional laminate failure mechanisms may not bear any resemblance to failure of multidirectional laminates. Thus, if failure mechanisms observed in such laminates (used to characterize the models herein) are extrapolated to predict failure in multiangle laminates (used in service), then the conclusions drawn from such an exercise may not represent an accurate evaluation of the predictive capabilities of such a model. It is hoped that in future studies a concurrent experimental and model building block approach will be undertaken to evaluate the true capability of multiscale analysis methodologies.

References

1. Bogetti, Travis A., et al.: Predicting the Nonlinear Response and Failure of Composite Laminates: Correlation With Experimental Results. Compos. Sci. Technol., vol. 64, 2004, pp. 477–485.
2. Paley, M.; and Aboudi, J.: Micromechanical Analysis of Composites by the Generalized Cells Model. Mech. Mater., vol. 14, no. 2, 1992, pp. 127–139.
3. Aboudi, Jacob; Arnold, Steven M.; and Bednarcyk, Brett A.: Micromechanics of Composite Materials: A Generalized Multiscale Analysis Approach. Elsevier, Boston, MA, 2013.
4. Bednarcyk, Brett A.; Aboudi, Jacob; and Arnold, Steven M.: Micromechanics Modeling of Composites Subjected to Multiaxial Progressive Damage in the Constituents. AIAA J., vol. 48, no. 7, 2010, pp. 1367–1378.
5. Pineda, Evan Jorge; Bednarcyk, Brett A.; and Arnold, Steven M.: Achieving ICME With Multiscale Modeling: The Effects of Constituent Properties and Processing on the Performance of Laminated Polymer Matrix Composite Structures. Presented at the 55th AIAA/ASME/ASCE/AHS/ASC Structures, Structural Dynamics, and Materials Conference, National Harbor, MD, 2014.
6. Sicking, Dean Leo: Mechanical Characterization of Nonlinear Laminated Composites With Transverse Crack Growth. Ph.D. Thesis, Texas A&M University, 1992.
7. Schapery, R.A.: A Theory of Mechanical Behaviour of Elastic Media With Growing Damage and Other Changes in Structure. J. Mech. Phys. Solids, vol. 38, no. 2, 1990, pp. 215–253.
8. Lamborn, M.J., and Schapery, R.A.: An Investigation of Deformation Path-Independence of Mechanical Work in Fiber-Reinforced Plastics. J. Compos. Mater., vol. 27, no. 4, 1993, pp. 352–382.
9. Wilt, T.E.: On the Finite Element Implementation of the Generalized Method of Cells Micromechanics Constitutive Model. NASA/CR—1995-195451, 1995. http://ntrs.nasa.gov
10. Pineda, Evan J., et al.: Progressive Damage and Failure Modeling in Notched Laminated Fiber Reinforced Composites. Int. J. Fracture, vol. 158, no. 2, 2009, pp. 125–143.
11. Engelstad, S.P., et al.: Assessment of Composite Damage Growth Tools for Aircraft Structure—Part I. AIAA 2015–1876, 2015.
12. Budiansky, B.; and Fleck, N.A.: Compressive Failure of Fibre Composites. J. Mech. Phys. Solids, vol. 41, no. 1, 1993, pp. 183–211.
13. Basu, Shiladitya; Waas, Anthony M.; and Ambur, Damodar R.: Prediction of Progressive Failure in Multidirectional Composite Laminated Panels. Int. J. Solids Struct., vol. 44, 2007, pp. 2648–2676.
14. Dassault Systèmes Simulia Corp.: Abaqus Analysis User's Manual. Vols. 1–3, Version 6.11-1, Dassault Systèmes Simulia Corp., Providence, RI, 2011.
15. Pineda, Evan J., et al.: Progressive Failure of a Unidirectional Fiber-Reinforced Composite Using the Method of Cells: Discretization Objective Computational Results. Int. J. Solids Struct., vol. 50, 2013, pp. 1203–1216.
16. Pineda, Evan, et al.: On Multiscale Modeling Using the Generalized Method of Cells: Preserving Energy Dissipation Across Disparate Length Scales. CMC-Comput. Mater. Con., vol. 35, no. 1, 2012, pp. 119–154.
17. Pineda, Evan J., et al.: Implementation of a Smeared Crack Band Model in a Micromechanics Framework. NASA/TM—2012-217603, 2012. http://ntrs.nasa.gov

18. Bazant, Zdenek P.; and Cedolin, Luigi: Blunt Crack Band Propagation in Finite Element Analysis. J. Eng. Mech.-ASCE, vol. 105, no. 2, 1979, pp. 297–315.
19. Pietruszczak, St.; and Mroz, Z.: Finite Element Analysis of Deformation of Strain-Softening Materials. Int. J. Numer. Meth. Eng., vol. 17, no. 3, 1981, pp. 327–334.
20. de Borst, R.: Computation of Post-Bifurcation and Post-Failure Behavior of Strain-Softening Solids. Comput. Struct., vol. 25, no. 2, 1987, pp. 211–224.
21. Krueger, Ronald, et al.: Comparison of 2D Finite Element Modeling Assumptions With Results From 3D Analysis for Composite Skin-Stiffener Debonding. Compos. Struct., vol. 57, 2002, pp. 161–168.
22. Yao, Q.; and Qu, J.: Three-Dimensional Versus Two-Dimensional Finite Element Modeling of Flip-Chip Packages. J. Electron. Packaging, vol. 121, no. 3, 1999, pp. 196–201.
23. Cameron, Kenneth D., et al.: Orbiter Kevlar/Epoxy Composite Overwrapped Pressure Vessel Flight Rationale Technical Assessment Report. NASA/TM—2009-215719/Volume I (NASA NESC–RP–07–34), 2007. Available from the NASA STI Program.
24. Cameron, Kenneth D., et al.: Shelf Life Phenomenon and Stress Rupture Life of Carbon/Epoxy Composite Overwrapped Pressure Vessels (COPVs). NASA/TM—2009-215714/Volume I (NESC–RP–06–83/04–009–E), 2009. Available from the NASA STI Program.
25. Weibull W.: The Phenomenon of Rupture in Solids. The Royal Swedish Institute for Engineering Research Proceedings, Ingenioersvetenskaps Akad. Handl., no. 153, 1939, pp. 1–55.
26. Bazant, Zdenek P.: Scaling of Structural Strength. Elsevier Science & Technology, Oxford, UK, 2005.
27. Satyanarayana, Arunkumar, et al.: Influence of Finite Element Size in Residual Strength Prediction of Composite Structures. AIAA 2012–1619, 2012.